Alpine thermal and structural evolution of the highest external crystalline massif: The Mont Blanc

P. H. Leloup,[1] N. Arnaud,[2] E. R. Sobel,[3] and R. Lacassin[4]

Received 5 May 2004; revised 14 October 2004; accepted 15 March 2005; published 1 July 2005.

[1] The alpine structural evolution of the Mont Blanc, highest point of the Alps (4810 m), and of the surrounding area has been reexamined. The Mont Blanc and the Aiguilles Rouges external crystalline massifs are windows of Variscan basement within the Penninic and Helvetic nappes. New structural, $^{40}Ar/^{39}Ar$, and fission track data combined with a compilation of earlier P-T estimates and geochronological data give constraints on the amount and timing of the Mont Blanc and Aiguilles Rouges massifs exhumation. Alpine exhumation of the Aiguilles Rouges was limited to the thickness of the overlying nappes (~10 km), while rocks now outcropping in the Mont Blanc have been exhumed from 15 to 20 km depth. Uplift of the two massifs started ~22 Myr ago, probably above an incipient thrust: the Alpine sole thrust. At ~12 Ma, the NE-SW trending Mont Blanc shear zone (MBsz) initiated. It is a major steep reverse fault with a dextral component, whose existence has been overlooked by most authors, that brings the Mont Blanc above the Aiguilles Rouges. Total vertical throw on the MBsz is estimated to be between 4 and 8 km. Fission track data suggest that relative motion between the Aiguilles Rouges and the Mont Blanc stopped ~4 Myr ago. Since that time, uplift of the Mont Blanc has mostly taken place along the Mont Blanc back thrust, a steep north dipping fault bounding the southern flank of the range. The "European roof" is located where the back thrust intersects the MBsz. Uplift of the Mont Blanc and Aiguilles Rouges occurred toward the end of motion on the Helvetic basal décollement (HBD) at the base of the Helvetic nappes but is coeval with the Jura thin-skinned belt. Northwestward thrusting and uplift of the external crystalline massifs above the Alpine sole thrust deformed the overlying Helvetic nappes and formed a backstop, inducing the formation of the Jura arc. In that part of the external Alps, ~NW-SE shortening with minor dextral NE-SW motions appears to have been continuous from ~22 Ma until at least ~4 Ma but may be still active today. A sequential history of the alpine structural evolution of the units now outcropping NW of the Pennine thrust is proposed. **Citation:** Leloup, P. H., N. Arnaud, E. R. Sobel, and R. Lacassin (2005), Alpine thermal and structural evolution of the highest external crystalline massif: The Mont Blanc, *Tectonics*, *24*, TC4002, doi:10.1029/2004TC001676.

1. Introduction

[2] Similar to most other collisional mountain belts, the Alps formed as a crustal-scale orogenic wedge [e.g., *Mattauer*, 1986], in this case above the southward continental subduction of Eurasia below Apulia (Figure 1b). The southward plunging slab has been imaged on ECORS and NFP20-west seismic reflection profiles down to a depth of ~40 km below the internal zones [e.g., *Nicolas et al.*, 1990; *Pfiffner et al.*, 1997]. Within the orogenic wedge, the thrusts propagated northwest toward the European foreland with a succession of flats and ramps (Figure 1b). In such a framework, the external crystalline massifs (ECM), which underlie most of the highest summits of the Alps with altitudes over 4000 m, have been interpreted as recent culminations above of a crustal thrust ramp [e.g., *Ménard and Thouvenot*, 1987; *Butler*, 1985; *Lacassin et al.*, 1990]. This paper focuses on the highest of the ECM: the Mont Blanc massif, the "European roof", which towers at 4810 m above all other alpine summits. Surprisingly, the alpine age structure of the highest alpine peak is still disputed, and this has important bearings on alpine deformation kinematics and mechanics as a whole.

[3] For some, the Mont Blanc is a coherent, crustal-scale sheet limited by faults or shear zones, and located in the hanging wall of an alpine thrust [e.g., *Bellière*, 1956; *Eltchaninoff-Lancelot et al.*, 1982; *Butler*, 1985]. The sedimentary cover rocks above and in front of the Mont Blanc massif would be separated from the basement by décollement zones and affected by thin-skinned folds and thrusts. For others, the Mont Blanc massif corresponds to a crustal-scale recumbent anticline forming the core of the Helvetic nappes [e.g., *Ramsay*, 1981; *Epard*, 1986; *Escher et al.*, 1988]. This would imply no significant differential slip between basement and cover. Such differing structural interpretations correspond to divergent views about the mechanical behavior of continental crust in orogens. Addi-

[1]Laboratoire des Sciences de la Terre, UMR CNRS 5570, Ecole Normale Supérieure, Université Claude Bernard, Villeurbanne, France.
[2]Laboratoire de Dynamique de la Lithosphère, UMR CNRS 5573, ISTEEM-USTL, Montpellier, France.
[3]Institut für Geowissenschaften, Universität Potsdam, Potsdam, Germany.
[4]Laboratoire de Tectonique, Mécanique de la Lithosphère, UMR CNRS 7578, Institut de Physique du Globe de Paris, Paris, France.

0278-7407/05/2004TC001676$12.00

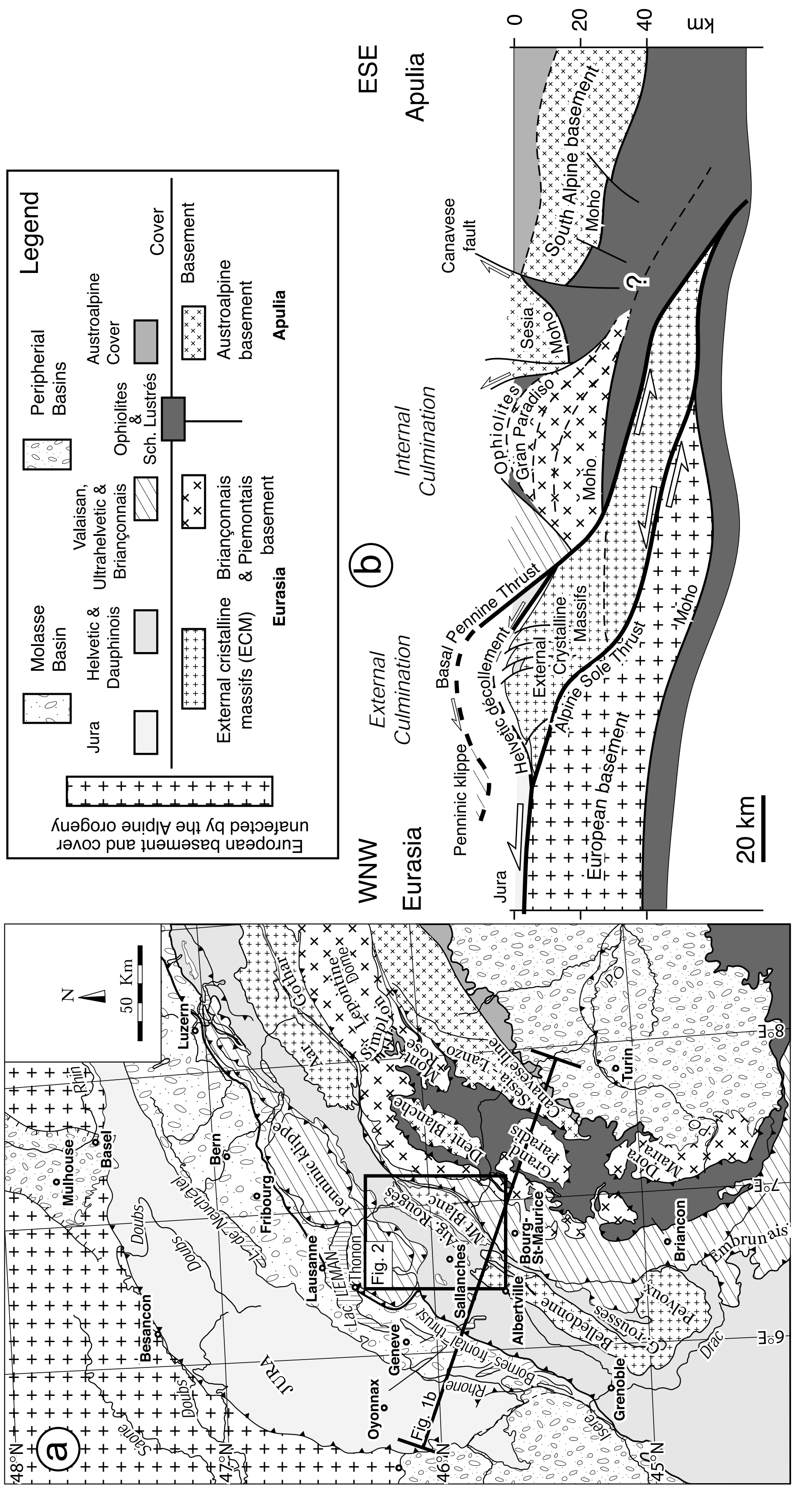

Figure 1. Structural framework of the western Alps. Legend is for both Figures 1a and 1b. (a) Structural map of the western Alps. (b) Large-scale geological cross section of the western Alps. Modified from *Lacassin et al.* [1990]. See color version of this figure at back of this issue.

tionally, some authors ascribe the high elevation of the range to an active normal fault bounding its SE flank [*Seward and Mancktelow*, 1994; *Lemoine et al.*, 2000] or emphasize the role of Tertiary strike-slip tectonics [*Gourlay*, 1983; *Hubbard and Mancktelow*, 1992]. Finally, in spite of the topographic evidence for recent and strong uplift, thus probably of exhumation, the importance of Tertiary metamorphism and of ductile deformations in presently outcropping rocks has generally been set aside.

[4] Our goal is thus to better understand how and when the Mont Blanc massif reached high elevations, and what this tells us about exhumation processes in mountain belts.

2. Overview of Mont Blanc Geology

[5] The Mont Blanc and Aiguilles Rouges massifs are two of the Alpine external crystalline massifs (ECM) that form a discontinuous belt along the periphery of the Alps (Figure 1). The ECM are located in the footwall of the Penninic basal thrust.

[6] The Mont Blanc massif is mostly composed of a calc-alkaline granite (Figure 2), locally called "Protogine" that constitutes the famous needles of the "Aiguilles de Chamonix". This granite has been dated by Rb/Sr at 316 ± 19 Ma [*Bussy et al.*, 1989] and by U/Pb on zircons at 304 ± 3 Ma [*Bussy and Von Raumer*, 1993]. The granite and related aplitic veins intrude Variscan metamorphic rocks (Figure 3b) comprising orthogneisses, paragneisses, carbonate lenses, mafic schists, and amphibolites [*Von Raumer and Neubauer*, 1993]. In these rocks, the foliations are generally steep and affected by isoclinal folds. To the NW, the Mont Blanc massif is separated from the Aiguilles Rouges massif by a strip of Mesozoic sedimentary rocks, commonly called "the Chamonix syncline", outcropping in the Chamonix glacial valley (Figure 2a). The Aiguilles Rouges are mostly composed of Variscan metamorphic rocks and granites encompassing synclines containing Visean and Westphalian sedimentary rocks (Figure 2) [*Pairis et al.*, 1993; *Bellière et al.*, 1987]. The NE-SW direction of the ranges is probably partly inherited from Mesozoic normal faults associated with the rifting of the alpine ocean [e.g., *Eltchaninoff-Lancelot et al.*, 1982; *Gillcrist et al.*, 1987]. The Triassic unconformity is clearly visible in the Aiguilles Rouges and at the northern and southern tips of the Mont Blanc massif (Figure 2a). NW of the Aiguille Rouges the Mesozoic sedimentary series of the subalpine domain is folded above a thick décollement level located in the Liassic black shales. As it has been tilted northwestward by the rise of the Aiguilles Rouges–Mont Blanc antiformal culmination, the present-day geometry of the décollement resembles that of a listric normal fault (Figure 2b). Laterally toward the NE, this décollement corresponds to the lower limit of the Helvetic nappe stack (Figure 2), the roots of which have to be found in the Chamonix valley [*Ayrton*, 1980; *Ramsay*, 1981] and/or in the Swiss Val Ferret SE of the Mont Blanc [*Grasmück*, 1961]. Along the SE flank of the Val Ferret, the Penninic basal thrust is a complex zone of stacked thrusts constituting the basal limit of the Penninic nappes. The roots of the Penninic klippes (Figures 1 and 2) are found in this zone [e.g., *Masson*, 1976]. Thus the Mont Blanc and Aiguille Rouges massifs correspond to a basement window within the Alpine sedimentary nappe stack.

3. Alpine Structures Within the Mont Blanc and Aiguilles Rouges Massifs

[7] Each of the three steep flanks that bound the Mont Blanc massif is associated with an alpine structure: the root of the Helvetic nappes to the east, the Mont Blanc back thrust to the south and the Mont Blanc shear zone to the northwest. The topography of the Aiguilles Rouges is more subdued and Alpine deformation is documented by the doming of the Triassic unconformity.

3.1. Roots of the Helvetic Nappes in the Val Ferret

[8] To the east, the Swiss flank of the Mont Blanc massif mostly corresponds to structural surfaces of Triassic sandstones lying unconformably on the granite (Figure 2). Intensively sheared Mesozoic slates overlie the Triassic rocks. Within the slates, the schistosity strikes N22°, 65°SE on average and carries a well-defined stretching lineation striking N134°, 65°SE on average (Figures 3c and 4a). The slates are affected by recumbent folds verging to the NW [*Ayrton*, 1969], consistent with shear criteria indicating a top to the NW sense of shear (Figure 3d). In some places "a" type and sheath folds testify to the intensity of shearing along what we will call the Val Ferret thrust. Toward the south, this thrust becomes slightly oblique to the stratigraphy and affects the granite (Figure 2 and Figure 4a). Farther to the north, in the Mont Chemin area, 5 km southeast of Martigny, thrusting has occurred along the Triassic unconformity, and dismembered Permo-Triassic sediments form a sliver between the Variscan gneisses and the Mesozoic sheared rocks (Figures 2a and 5a). Cartographically, the Val Ferret thrust continues to the north and, disappears beneath the thick Quaternary infill of the Rhône valley. North of that valley, the most probable equivalent of this thrust is the basal contact of the Morcles nappe (Figure 2a).

3.2. Mont Blanc Back Thrust

[9] Between the Mont Blanc de Courmayeur and the Grandes Jorasses the southwestern flank of the range is impressively steep (average slope of 35° from the top of the Mont Blanc de Courmayeur to the Val Veni over 3000 m below). It is marked by several steeply northward dipping thrust faults (Figure 2a). The southernmost thrust brings the Mont Blanc granite on top of the Jurassic-Cretaceous sedimentary series [e.g., *Baggio*, 1964; *Antoine et al.*, 1975; *Guermani and Pennacchioni*, 1998]. Northeast of Courmayeur, near Pra Sec, the thrust dips 55° to the NW (Pr on Figure 6), is marked by a ~2 m thick fault breccia and brings the granite on top of black schists and Cretaceous sandy limestones that were previously interpreted as lying unconformably on the granite [*Antoine et al.*, 1975, 1979]. Farther SW, below the Boccalatte refuge and near the Mont Fretty the contact dips 50–65° to the NW and brings the

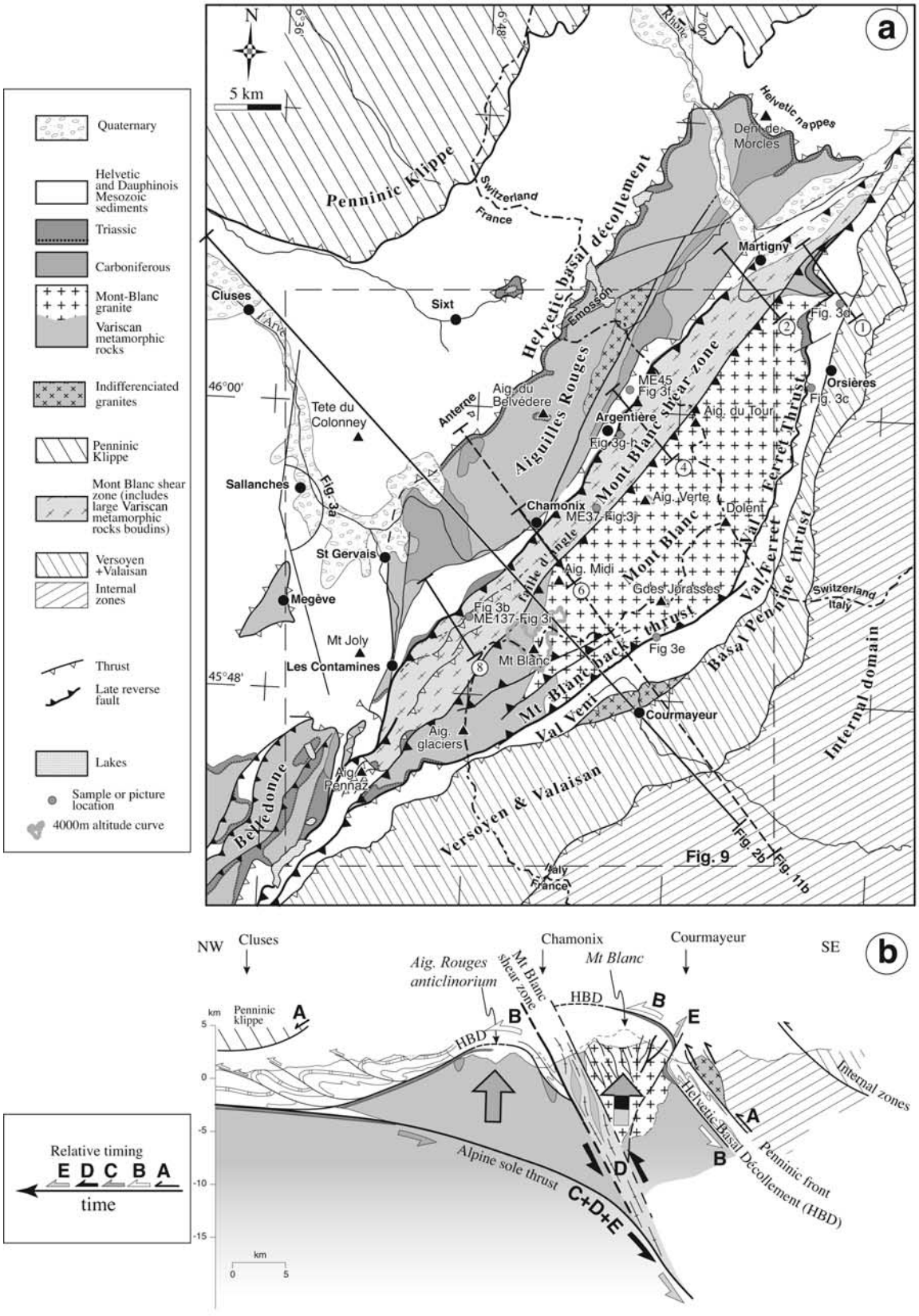
a
N
5 km
6°36'
6°48'
7°00'
Rhône
Quaternary
Helvetic and Dauphinois Mesozoic sediments
Triassic
Carboniferous
Mont-Blanc granite
Variscan metamorphic rocks
Indifferenciated granites
Penninic Klippe
Mont Blanc shear zone (includes large Variscan metamorphic rocks boudins)
Versoyen +Valaisan
Internal zones
Thrust
Late reverse fault
Lakes
Sample or picture location
4000m altitude curve
Penninic Klippe
Switzerland
France
Helvetic nappes
Dent de Morcles
Helvetic basal décollement
Martigny
Cluses
Sixt
Arve
Emosson
Fig. 3d
Orsières
Fig. 3c
ME45 Fig 3f
Aig. du Belvédere
Aig. du Tour
Argentière
Fig 3g
Aiguilles Rouges
Mont Blanc shear zone
Val Ferret Thrust
46°00'
Tete du Colonney
Anterne
Sallanches
Fig. 3a
Chamonix
ME37 Fig 3j
Aig. Verte
Dolent
St Gervais
Aig. Midi
Mont Blanc
Val Ferret thrust
Vallée d'Angle
Megève
Fig 3b
ME137 Fig 3i
Gdes Jorasses
Switzerland
Italy
Mt Joly
Les Contamines
Mt Blanc
Fig 3e
Basal Penninic thrust
45°48'
Mt Blanc Back thrust
Val Veni
Courmayeur
Aig. glaciers
Internal domain
Aig. Rennaz
Belledonne
Versoyen & Valaisan
Fig. 9
Fig. 2b
Fig. 11b
Italy
France
b
NW
Cluses
Chamonix
Courmayeur
SE
Aig. Rouges anticlinorium
Mt Blanc shear zone
Mt Blanc
Penninic klippe
HBD
Internal zones
Helvetic-Basal Décollement (HBD)
Penninic front
Alpine sole thrust
C+D+E
km
Relative timing
E D C B A
time

Figure 2

granite on top of overturned Liassic slates. These series probably correspond to the roots of the Helvetic nappes in the hanging wall of the Val Ferret thrust but overturned below a counter thrust: the Mont Blanc back thrust (Figure 2). The contact is well exposed on the trail to the Boccalatte refuge where it corresponds to a ~50 m thick granite cataclasite layer (Figure 3e). West of Mont Fretty, within the granite numerous greenschist shear zones anastomose around less deformed lenses [*Guermani and Pennacchioni*, 1998]. Most mylonitic shear zones trend N16° to N52° and display shear criteria suggesting top to the SE (dip slip) thrusting. However, given the common absence of stretching lineations and the strong influence of preexisting brittle faults on the shear zones geometry [*Guermani and Pennacchioni*, 1998], the precise direction of thrusting is difficult to constrain. The brittle faults that affect the granite show chlorite crystallization, are mostly parallel to the Mont Blanc back thrust and often show dip slip motions (Figure 6). Northwest of Courmayeur, near Peuterey village, the fault contact strikes N36°, is nearly vertical (P on Figure 6), and shows evidence for upward motion of the northwestern (Mont Blanc) unit. Within the granite, ~2 km away from the main contact, two major shear zones straddle the Aiguille de la Brenva (Figure 2a) and probably merge at depth to form the major NW dipping shear zone found in the Mont Blanc tunnel 3.5 km from the Italian entrance. The northernmost shear zone outcrops near the Helbronner cable car station and exhibits a clear morphological trace through the Peuterey and Rey passes, at the base of the highest part of the Mont Blanc massif (Figure 2a). In the deformed sedimentary series of the Val Veni, few brittle faults that reactivate schistosity planes show dextral motion (Figure 6).

3.3. Mont Blanc Shear Zone

[10] The northwestern flank of the Mont Blanc massif corresponds to the edge of the Chamonix valley deeply carved by the glaciers within the stripe of Mesozoic sediments pinched between the Mont Blanc and the Aiguilles Rouges. These sediments are deformed and locally overturned below the Mont Blanc granite and the Variscan gneisses (Figure 5e). Early workers interpreted this geometry as indicative of Alpine thrusting of the Mont Blanc basement on top of the Mesozoic series and of the Aiguilles Rouges massif [e.g., *Bellière*, 1956; *Eltchaninoff-Lancelot et al.*, 1982; *Butler*, 1985; *Gourlay*, 1986]. Within the Mont Blanc basement rocks, the contact is marked by an up to 4 km wide zone of heterogeneously deformed mylonitic rocks, interpreted as due to Tertiary thrusting of the Mont Blanc [*Bellière*, 1956]. However, the same author later claimed that the mylonites were locally intruded by the Variscan Mont Blanc granite and unconformably covered by Mesozoic sediments [*Bellière*, 1988]. He thus restricted the alpine deformation to a single brittle fault named the ''Faille d'Angle'' (Figure 2a). For others, the contact between the Mont Blanc basement and the Mesozoic series is an overturned unconformity [e.g., *Epard*, 1986]. Our study refutes these later views and confirms the existence of a Tertiary reverse shear zone fringing the Mont Blanc to the NW: the Mont Blanc shear zone (MBsz, Figures 2 and 5). If it is true that the Mont Blanc granite and related dikes intrude Variscan metamorphic rocks, all these rocks are deformed in the MBsz that we describe in more details below.

[11] From Sembrancher (NE) to the Jovet pass (SW), the MBsz is marked by SE dipping greenschist foliations that affect the Mont Blanc granite and overprint the Variscan schists. This deformation was characterized in the field along 12 cross sections; five of these sections are taken to illustrate the overall structure (Figure 5). The greenschist foliation is marked by white micas, chloritized biotites, and chlorite (Figure 3j). The foliation anastomoses around boudins of Variscan gneisses free of any greenschist deformation. Within these boudins, aplitic dikes, similar to those found in the Mont Blanc granite, crosscut the Variscan age foliation (Figure 3b), while outside of the boudins, the dikes are affected by the mylonitic deformation (Figure 3h). Around the boudins, the greenschist foliation trends N355° to N80° (N35°, 48°E on average; Figure 4d) and bears a steep mineral and stretching lineation with pitches between 90° and 70°NE (average direction: N110°, 50°E; Figures 3g and 4d). Shear criteria in the mylonites (mostly C/S relationships) consistently indicate a top to the NW (thrusting) sense of shear (Figures 3h, 3i, and 3j). Near Le Tour, the Mesozoic sediments that structurally underlie the Mont Blanc gneisses (Figure 5c) show schistosities and a stretching lineation (e.g., ME45, schistosity N24°, 60°E, lineation pitch 78°N) parallel to the gneissic mylonites (Figures 4c and 4d). C/S relationships within these rocks clearly indicate thrusting (Figure 3f). These field relationships imply that the greenschist metamorphism and deformation of the NW border of the Mont Blanc massif is of Alpine age. The kinematics of that deformation implies that the MBsz is a steep reverse ductile fault with a minor dextral component of movement.

[12] Toward the southwestern end of the Mont Blanc massif, the greenschist foliation tends to be shallower and exhibits less clear lineations. At the Col de Tricot, the Mesozoic sedimentary rocks just below the basement gneisses are mylonitic and show shear planes with white mica recrystallization. These mylonites are subparallel to the greenschist foliation in the overlying basement gneisses and to the axial plane cleavage in the underlying Mesozoic

Figure 2. Structure of the Mont Blanc massif. (a) Structural map of the Mont Blanc massif. The map is drawn from published geological maps: Mont Blanc [*Antoine et al.*, 1979]; Chamonix [*Bellière et al.*, 1987]; Cluses [*Pairis et al.*, 1993], and St. Gervais-les-Bains [*Mennessier et al.*, 1976], as well as personal observations. (b) Synthetic cross section of the Mont Blanc massif. On the basis of our observations (see also Figure 5), HBD is the Helvetic basal décollement. Note that this section is compatible with recent gravity data of the area [*Masson et al.*, 2002]. See section 3.6 for discussion on the relative timing of deformation events. See color version of this figure at back of this issue.

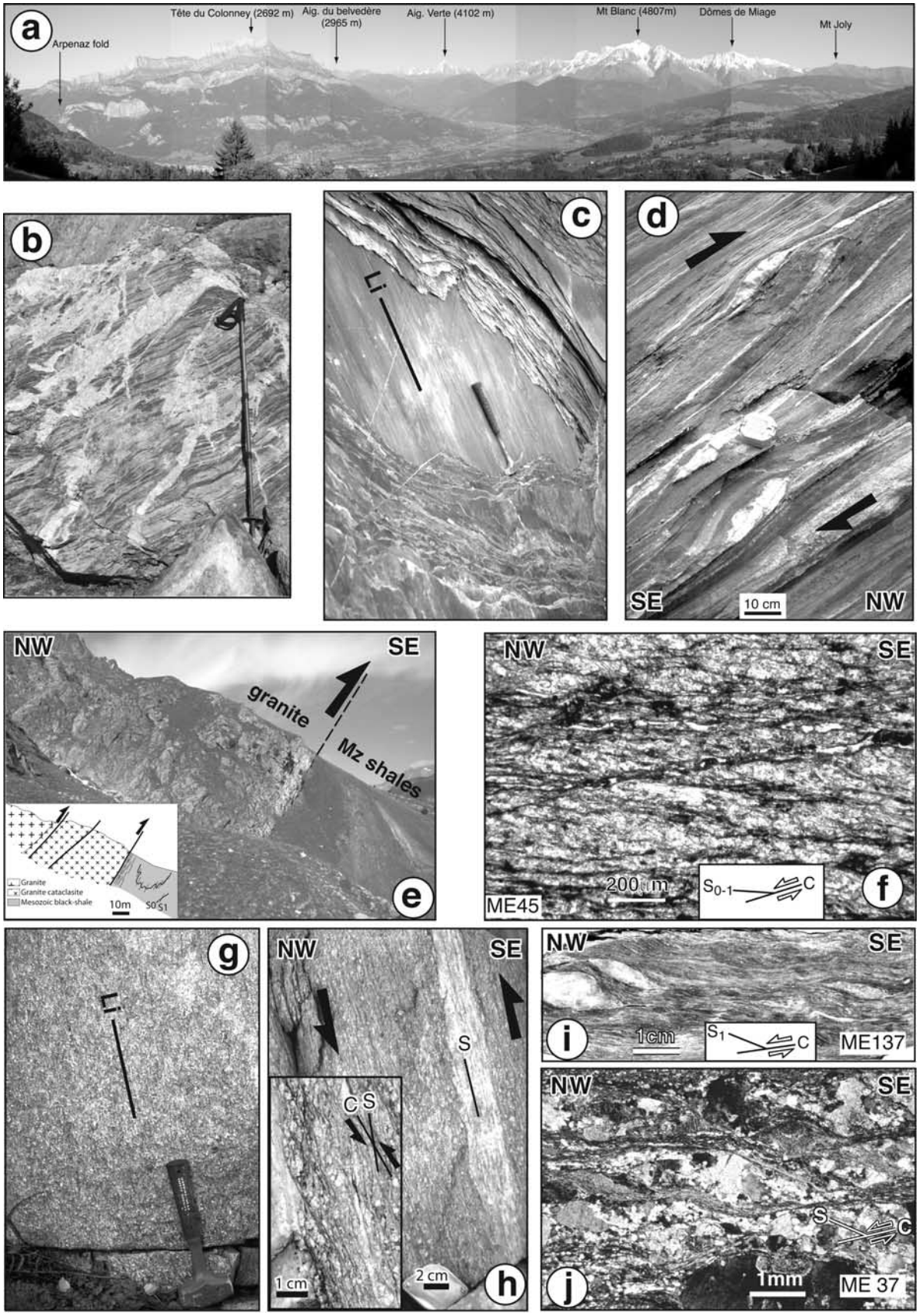
a
Arpenaz fold
Tête du Colonney (2692 m)
Aig. du belvedère (2965 m)
Aig. Verte (4102 m)
Mt Blanc (4807m)
Dômes de Miage
Mt Joly
b
c
Li
d
SE
10 cm
NW
NW
SE
granite
Mz shales
Granite
Granite cataclasite
Mesozoic black-shale
10m
S0
S1
e
NW
SE
200 µm
ME45
S0-1
C
f
g
Li
NW
SE
S
C S
1 cm
2 cm
h
NW
SE
1cm
S1
C
ME137
i
NW
SE
S
C
1mm
ME 37
j

Figure 3

rocks (Figure 5, section 8) [e.g., *Bellière*, 1956]. This relationship indicates alpine thrusting of the Mont Blanc basement on top of the Mesozoic sediments of the "Chamonix syncline" contrary to the conclusions of *Epard* [1986], who advocated for an inverted unconformity.

3.4. Deformation Within the Mont Blanc Granite

[13] Within the Mont Blanc granite, the preferred orientation of biotites, sometimes feldspars, and of restitic enclaves, marks a subvertical magmatic foliation striking NNE-SSW [*Von Raumer*, 1967]. Aplitic veins cut this foliation. Both the granite and the aplitic veins are affected by numerous greenschist shear zones and faults that postdate the magmatic foliation. Shear zone mylonites bear muscovite + green biotite + albite + chlorite ± epidote ± titanite [*Rolland et al.*, 2003], while the faults show either chlorite or epidote fiber crystallizations. The faults and shear zones have a large range of orientations but most trends NW-SE with an inverted fan geometry across the range. They are generally parallel to the MBsz to the NW and to the Mont Blanc back thrust to the SE [*Bertini et al.*, 1985] (Figure 2b). The granite is also affected by numerous horizontal tension gashes and veins filled with quartz crystallizations. These veins when open yield spectacular automorphic quartz crystals, they may also contain epidote, K-feldspar (adularia), fluorite, muscovite and calcite.

3.5. Aiguilles Rouges Massif

[14] The Aiguilles Rouges massif is mostly composed of Variscan gneisses and micaschists. A few granites, such as the 306 ± 1.5 Ma Vallorcine granite [*Bussy et al.*, 2001], intrude these rocks. Foliations are generally steep, strike N335° to N55° (N20° on average, Figure 4b) and are locally affected by isoclinal folds. When present, the lineation dips relatively shallowly, 22 to 55° to the north (Figure 4b). The Aiguilles Rouges also includes Late Carboniferous basins affected by Late Variscan deformations (Figure 2a). Triassic conglomerates and sandstones unconformably cover these basins as well as the metamorphic and granitic rocks (Figure 2a).

[15] The intensity of alpine deformation can be estimated by looking at the present-day geometry of the Triassic unconformity that describes a broad NE-SW dome (Figure 2b). The unconformity is mapped as horizontal at an elevation of ~2850 m, below the summit of the Aiguille de Belvédère (Figure 2a) [*Bellière et al.*, 1987], while on the northwestern flank of the Aiguilles Rouges it dips ~30°NW and is overlain by the Liassic décollement zone (for instance, near the Anterne and Emosson lakes). Farther NW, it is found at an elevation of 1200 m NE of Sixt (Figure 2) [*Pairis et al.*, 1993]. Outcrop-scale observations (for instance, above the Vieux Emossons lake) suggest that warping and small-scale folding of the unconformity is accommodated by distributed slip on the preexisting steep foliation planes in the basement rocks. Above the unconformity, the Liassic décollement zone fringes the whole northwestern flank of the Aiguilles Rouges massif and merges with the reverse limb of the Dent de Morcles recumbent fold, basal contact of the Helvetic nappe stack (Figure 2a). The entire Helvetic nappe stack has the same domal shape as the underlying Triassic unconformity [e.g., *Pfiffner*, 1993].

3.6. Summary and Relative Chronology of Alpine Deformations in the Mont Blanc–Aiguilles Rouges Area

[16] The first major Alpine deformation in the Mont Blanc area is the formation of the Penninic nappes above the Penninic basal thrust that ended in the upper Eocene [e.g., *Pfiffner et al.*, 2002] (A on Figure 2b). The structural observations presented above shed light on more recent deformation events in the footwall of the Penninic basal thrust.

[17] The geometry of the subalpine chain, the Helvetic nappes and the location of their roots, as well as the importance of NW vergent alpine thrusting of the Mont Blanc has been the subject of a lively debate. Mont Blanc thrusting is of major importance for some (e.g., ~50 km for *Ayrton* [1980] or more than 67 km for *Butler* [1985]), while it is nonexistent for others [e.g., *Epard*, 1986; *Gidon*, 2001]. The roots of the Helvetic nappes have been placed in the

Figure 3. Deformation in the Mont Blanc massif. For pictures locations see Figure 2a. (a) High glaciated peaks of the Mont Blanc massif viewed from the WNW; view from Cordon, above Sallanches. This landscape is an oblique view of the central part of the section shown in Figure 2b. (b) Aplitic veins intruding the Variscan gneisses; SW part of the Mont Blanc massif, above the Nid d'Aigle. (c) Schistosity and stretching lineation in Liassic shales in Combes des fonds of the Swiss Val Ferret, corresponding to the root of the Helvetic nappes. Li indicates the lineation direction (see Figure 4a). Hammer gives scale. (d) Sheared calcite veins in Liassic shales of the Swiss Val Ferret indicating top to the NW thrusting. Compass gives scale. (e) Back thrusting of the Mont Blanc granite on top of the steepened Liassic series of the Italian Val Ferret. Picture is from the pathway to the Bocallette refuge, south of the Grandes Jorasses. The inset is the corresponding cross section. (f) Thin section of Mesozoic calcschists of the Chamonix syncline. Vormaine ridge, near Le Tour (see Figure 5c). The rock shows a strong schistosity (N21°, 57°E) and lineation (pitch 72°N) (Figure 4c). The shear planes (C) indicate a top to the NW sense of shear parallel to motion in Mont Blanc shear zone (Figure 4c and 4d). (g) Alpine stretching lineation in othogneissess (Ordovician protolith) east of Argentière. Foliation is N15°, 67°E, and lineation pitch is 77°N (see Figure 4d). (h) Sheared aplitic vein in the Argentière orthogneisses. The inset shows C/S structures in orthogneiss. C planes shallower than the foliation indicate thrusting to the NW. (i) Polished slab of sample ME137 from an alpine shear zone affecting the Variscan gneiss. Foliation is N60°, 48°S, and lineation pitch is 75°E. C/S relationships indicate thrusting to the NW. (j) Thin section of sample ME37, Echelles du Montenvers. Foliation is N20°, 65°S, and lineation pitch is 90°. C/S relationships indicate thrusting to the NW. See color version of this figure at back of this issue.

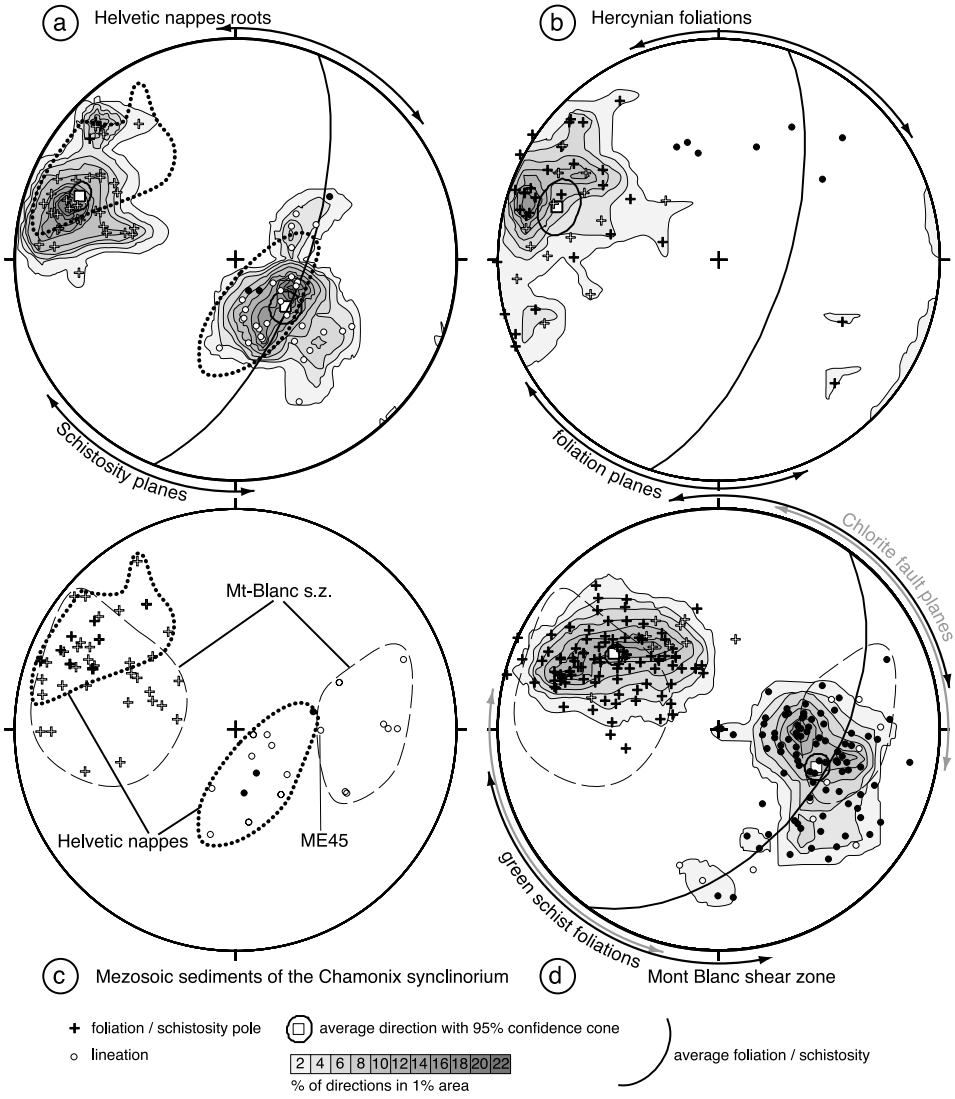

Figure 4. Structural data of the Mont Blanc massif. Schmidt lower hemisphere projection. (a) Schistosities and stretching lineations from the root zone of the Helvetic nappes. Measurements are along the Swiss Val Ferret, within Mesozoic sediments (open symbols) and the Mont Blanc granite (solid symbols). The average schistosity pole trends N292°, 25° (39 data, K = 26.2), corresponding to an average plane trending N22°, 65°E. The average lineation trends N134°, 64° (35 data, K = 17.5). The dotted lines refer to the range of data observed in the Chamonix synclinorium (see Figure 4c). (b) Variscan foliations. Foliations are ascribed to Variscan deformations s.l. (see text for details). These data include foliations of Paleozoic rocks within the Posette synclinorium (white symbols) (Figure 5c). The average foliation pole trends N288°, 25° (48 data, K = 6.5), corresponding to an average plane trending N48°, 65°E. Note that there are only a few lineations, most of them dipping shallowly. (c) Schistosities and lineations within the Mesozoic sediments of the Chamonix synclinorium. The two lineation and foliation groups are ascribed to two distinct structures: the tilted décollement at the base of the Helvetic nappes (dotted lines) and the Mont Blanc shear zone (long dashed lines). Solid symbols refer to shear planes affecting the Aiguilles Rouges basement. See text for details. (d) Mont Blanc shear zone. Foliations are ascribed to Alpine deformations within the Mont Blanc shear zone (see text for details). Data include medium temperature lineation from the NW flank of the Mont Blanc (solid symbols) as well as low-temperature lineations mostly from the Nid d'Aigle area (open symbols). The average foliation pole trends N306°, 42° (108 data, K = 15.5), corresponding to an average plane trending N36°, 48°E. The long dashed lines refer to the range of data observed in the Chamonix synclinorium (see Figure 4c).

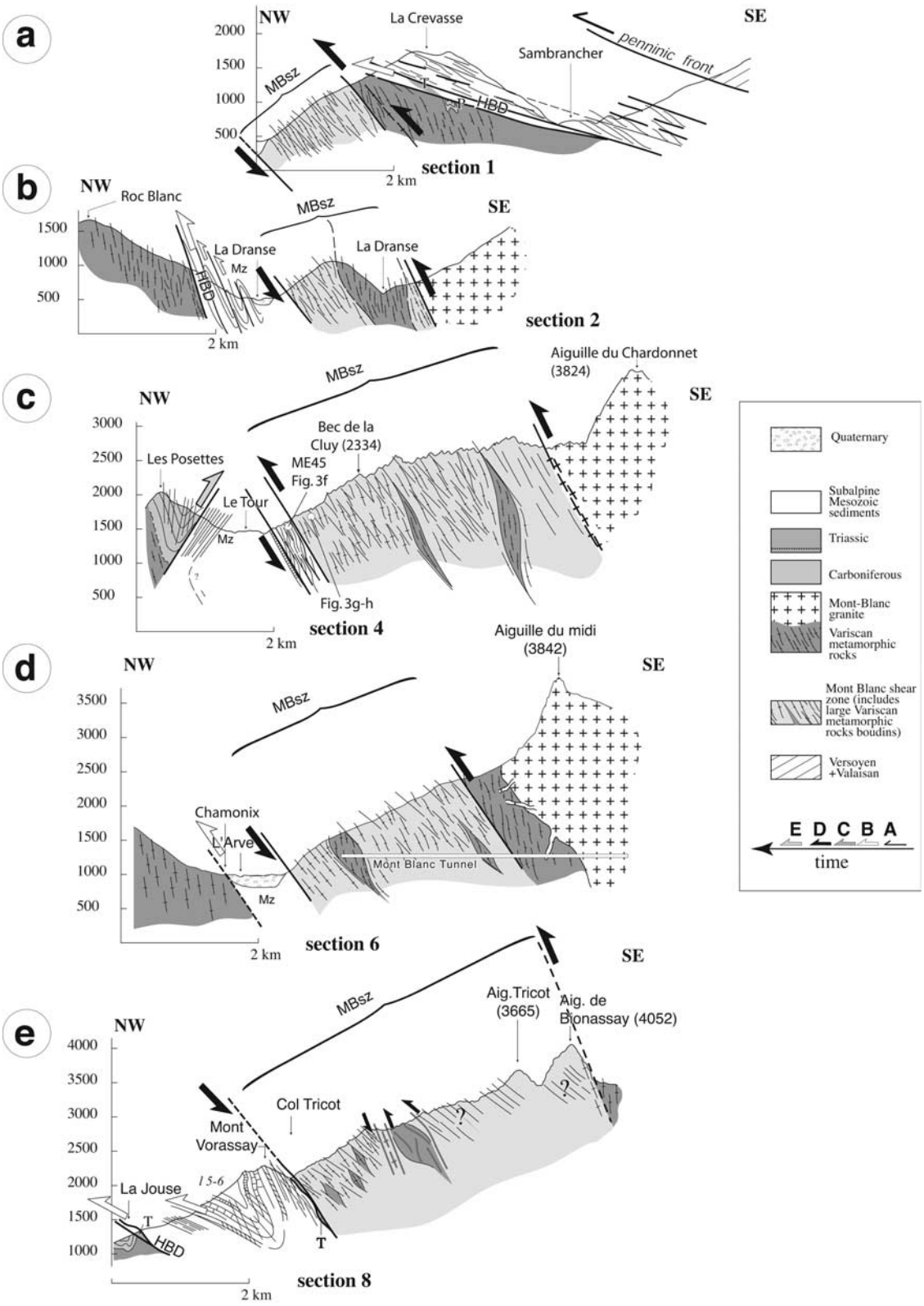

Figure 5. Cross sections of the NW flank of the Mont Blanc massif. NW-SE cross sections from the northern to the southern extremity of the massif (sections 1 to 8, respectively). See Figure 2a for locations. No vertical exaggeration. Mz and l 5–6 refer to Mesozoic sediments and T refers to Triassic sandstones. See color version of this figure at back of this issue.

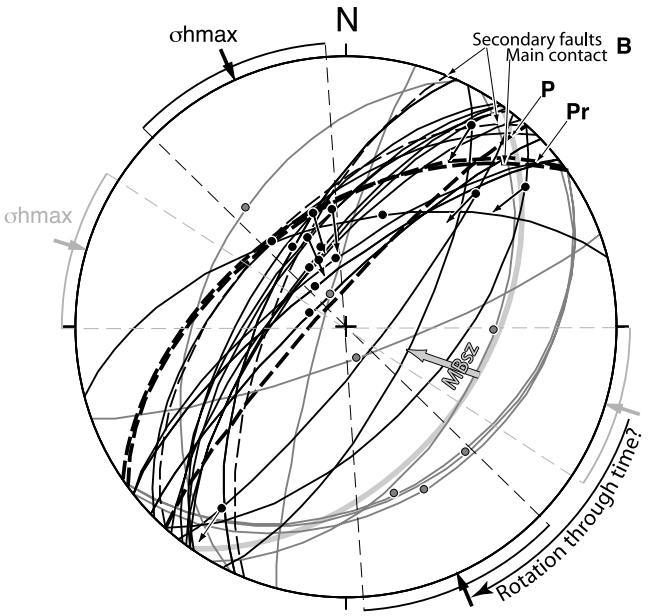

Figure 6. Brittle faults of NW flank (Nid d'Aigle) and SE flank of the Mont Blanc massif. Brittle faults from the Nid d'Aigle area are gray, while those from the SE flank of the massif are solid. Arrows mark the direction of motion of the upper block when it could be confidently determined. The Mont Blanc shear zone is shown in light gray for comparison. The thick dashed planes correspond to the contact between the granite and the sedimentary series along the Mont Blanc back thrust, below the Boccalatte refuge (B), near Pra Sec (Pr), and at Peuterey (P). The dextral strike-slip faults correspond to reactivated schistosity planes within Mesozoic sediments of the Val Ferret and Val Veni. The faults likely correspond to two and maybe three directions of the maximum horizontal stress (σhmax) (see text for details). This is a Schmidt lower hemisphere projection.

Chamonix synclinorium [*Ayrton*, 1980; *Eltchaninoff-Lancelot et al.*, 1982], within the Mont Blanc massif itself between an internal and an external Mont Blanc [e.g., *Epard*, 1990] or in the Val Ferret east of the Mont Blanc. Our structural observations show that the so-called "external" Mont Blanc corresponds to the Mont Blanc shear zone (MBsz). This steep reverse fault offsets the basal contact of the subalpine and Helvetic nappes (Figure 2b). In our interpretation, this contact, the basal contact of the Mesozoic sediments in the Chamonix synclinorium and the Val Ferret thrust, all correspond to the same major thrust: the Helvetic basal décollement (HBD), rooted east of the Mont Blanc. The HBD is refolded in a broad anticline above the Aiguilles Rouges and Mont Blanc basement culmination and is offset by the MBsz (Figure 2b). Deformations observed in the Mesozoic sediments of the Chamonix valley are thus related to two distinct structures: the HBD and the MBsz (Figure 4c).

[18] This implies that both the doming and uplift of the Aiguilles Rouges–Mont Blanc culmination (C on Figure 2b) and the initiation of the MBsz (D on Figure 2b) took place after overthrusting of the Helvetic nappes (B on Figure 2b). However, the relative timing between the doming and the MBsz remains unclear. We favor a scenario with doming of the Aiguilles Rouges taking place first, before out-of-sequence activation of the MBsz (Figure 2). Alternatively, the MBsz could have been active first, followed by propagation of deformation on a lower angle fault toward the NW. In that case, the MBsz would have been transported passively toward the NW.

[19] Along the southern extremity of the Mont Blanc, the Pennaz imbricates involve steeply dipping slices of deformed Mesozoic sediments. In that area, basement rocks of the Roselette klippe rest on top of Mesozoic sediments NW of the Pennaz imbricates. This geometry led *Butler* [1983] to propose a NW vergent flat thrust of the Mont Blanc. In a comment on *Butler*'s [1983] work, *Platt* [1984] proposed the existence of a late steep fault, termed "breach thrust". Our observations are more in accordance with *Platt*'s [1984] interpretation, with the Roselette klippe corresponding to a piece of basement rock involved within the HBD, latter cut by steep faults In the southern prolongation of the MBsz (Figure 2). In most areas of the Mont Blanc and Aiguilles Rouges massifs, the HBD sits just above the Triassic unconformity, but in other places it clearly cuts off basement rocks, as observed along the southern portion of the Val Ferret Thrust (Figure 2a). Such local involvement of the basement in the décollement level probably results from the existence of tilted blocks inherited from Mesozoic extension. The Pennaz imbricates that contain basement slices are thus probably steepened traces of the Helvetic décollement, partly reactivated by splays of the MBsz.

[20] Within the Mont Blanc granite, the crystallized gashes, and the postmagmatic shear zones, interpreted by all authors to be of Alpine age, are compatible with a ~NW-SE compressive stress with σ3 vertical. The detailed interpretation of the brittle faults is more complex. On both sides of the Mont Blanc, most brittle faults show dip-slip motion. These faults are most probably conjugate faults, implying a NNW-SSE maximum horizontal stress (σhmax) striking between N134 and N176 (Figure 6). These faults are parallel to the Mont Blanc back thrust (Figure 6), which thus appears to have formed under a NNW-SSE compressive stress regime. However, such compression would induce a reverse/sinistral motion on any NE-SW plane, and cannot explain the reactivation of few cleavage planes in dextral faults south of the Mont Blanc, nor the transport direction on the MBsz, which has a significant right-lateral component (Figure 6). It is thus very likely that at least two distinct directions of compression were present during the late evolution of the Mont Blanc massif: one oriented WNW-ESE during motion along the MBsz (D on Figure 2), and another oriented NNW-SSE during motion along the back thrust (E on Figure 2). The back thrust is probably the most recent of the two structures because (1) deformation on the back thrust is largely brittle suggesting an activation at a time when the granite had already been partly exhumed and (2) at the "Nid d'Aigle" on the

northern flank of the Mont Blanc, the brittle faults conjugated with the Mont Blanc back thrust are late with respect to the MBsz schistosity, and (3) the slope of the south flank of the range is exceptionally steep, even more than the north flank, suggesting recent and possibly still active uplift.

4. Constrains on the Amount and Timing of Alpine Metamorphism and External Crystalline Massifs Exhumation

4.1. Variscan and Alpine Metamorphisms

[21] The Aiguilles Rouges and the Mont Blanc massifs experienced at least two metamorphic phases: during the Variscan and the Alpine orogeny. After Variscan metamorphism and granitic intrusions, portions of both massifs were exposed at the surface prior to the deposition of Triassic sandstones.

[22] In the Aiguilles Rouges massif, a large part of the exhumation occurred before the deposition of Late Carboniferous (308–293 Ma) clastic and coal-bearing sediments [*Capuzzo and Bussy*, 1999; *Capuzzo et al.*, 2003]. Variscan P-T paths show high-pressure metamorphic conditions: up to 12 kbar [*Von Raumer et al.*, 1999]. In contrast, Alpine metamorphism is limited to the zeolite facies: pumpellyite-phrenite-clorite-titanite-albite-calcite-K-feldspar [*Von Raumer*, 1974]. On the basis of illite crystallinity, alpine metamorphism at the base of the Helvetic nappes, and thus at the top of Aiguilles Rouges and Mont Blanc basement, belongs to the epizone (greenschist facies) [*Aprahamian*, 1988]. This is confirmed by $\delta^{18}O$ measurements in syntectonic veins of the Morcles nappe suggesting temperatures of 350 ± 20°C at the beginning of the deformation (Figure 7) with a slight decrease of temperature (30–50°C) during deformation [*Kirschner et al.*, 1995].

[23] In the Mont Blanc, the only P-T data attributed to the Variscan metamorphic episode comes from its NE extremity, and indicate isobaric cooling at medium pressure and temperatures (6 ± 1 kbar and 550 ± 40 to 450 ± 50°C [*Marshall et al.*, 1997]). The Mont Blanc granite emplacement depth has been estimated as between 4 and 14 km (1 to 3.8 kbar) [*Marshall et al.*, 1997; *Bussy*, 1990]. The occurrence of microgranular facies, and rhyolites on the NE flank of the massif underneath the Triassic unconformity [*Bonin et al.*, 1993; *Bussy et al.*, 2001] show that at least this part of the massif was exhumed prior to the Triassic. However, alpine metamorphism was stronger in the Mont Blanc than in the Aiguilles Rouges. It induced crystallization of greenschist minerals: actinote, green biotite, chlorite, epidote, albite and titanite, and more locally, hornblende, zoïsite, clinozoïsite, and white mica [*Von Raumer*, 1974]. White micas crystallized in shear planes of Alpine mylonites that deform the Variscan gneisses, the Mont Blanc granite and the Mesozoic cover rocks. Within the granite, mucovite-chlorite equilibria in a muscovite+biotite+chlorite+epidote bearing shear zone gives P-T estimates of 0.5 ± 0.05 GPa and 400 ± 25°C [*Rolland et al.*, 2003] (10, Figure 7). Alpine P-T conditions are also constrained by microthermometric studies of fluid inclusions within minerals (mostly quartz) hosted by alpine veins (1 to 9, Figure 7) [*Poty et al.*, 1974; *Poty and Cathelineau*, 1999; *Fabre et al.*, 2002; *Marshall et al.*, 1998b]. All of the P-T estimates are combined in Figure 7 to define the alpine exhumation path of the Mont Blanc rocks. The temperatures culminate at ~400°C, in good agreement with estimates from the base of the Morcles nappe (Figure 7).

4.2. Existing Geochronological Constrains

[24] Two $^{40}Ar/^{39}Ar$ hornblende ages (≥334 and 309 ± 6 Ma) at the northeastern extremity of the Mont Blanc have been interpreted as maximum ages for the Variscan metamorphism, probably linked with granite emplacement [*Marshall et al.*, 1997]. The ages of the Mont Blanc granite itself (303 ± 2 Ma [*Bussy and Von Raumer*, 1993] and of several magmatic and anatectic rocks of the Aiguilles Rouges (between 332 and 306 Ma) are well constrained by U-Pb ages on zircons and monazites [*Bussy et al.*, 2001].

[25] Within the Mont Blanc granite, *Baggio et al.* [1967] were the first to describe and date secondary biotite crystallization, mostly from shear zones. Their Rb/Sr ages span between 18 and 36 Ma (Figure 8), but because initial Sr values were assumed to be that of the whole rock analysis (Sr_i = 0.726), these ages are disputable. However, they reveal alpine recrystallization and/or strong reheating. Another approach has been K/Ar dating of adularia K-feldspar and muscovite within the alpine veins. Ages range from 15.2 to 18.3 for adularia and 13.4 to 15.2 for muscovite [*Leutwein et al.*, 1970] (Figure 8). The corresponding Rb/Sr ages are anomalously old for adularia while a muscovite gives 14.8 Ma [*Leutwein et al.*, 1970]. A muscovite from a gold-bearing quartz vein shows excess argon and yields a 9.9 ± 1 Ma $^{40}Ar/^{39}Ar$ isochron age [*Marshall et al.*, 1998a]. This suggests that most K/Ar ages from vein minerals are maximum ages. Muscovites and microcline from two different mylonites yielded 40 ± 3 Ma [*Leutwein et al.*, 1970] and 41 ± 1 Ma [*Krummenacher and Evernden*, 1960] K/Ar ages, respectively, almost identical to the 46.5 ± 1.9 Ma $^{40}Ar/^{39}Ar$ age from paragonites of paragonite-keratophyre schists in northeastern Mont Blanc [*Marshall et al.*, 1998b]. This large distribution in age, revealing either multiple events or disequilibria in the chronometric systems, and the evidence for massive fluid circulation during the alpine deformation [e.g., *Rolland et al.*, 2003; *Rossi et al.*, 2005], suggests that additional $^{40}Ar/^{39}Ar$ data would be useful.

[26] The age of the subalpine (Helvetic) nappe stack emplacement (event B, Figure 2b) appears to be well constrained between 32 and ~15 Ma (Figure 8). The Taveyannaz volcaniclastic sandstones that were deposited prior to the nappe stacking contain 32.5 Ma andesitic clasts ($^{40}Ar/^{39}Ar$ on hornblendes), while biostratigaphic correlations suggest sedimentation between ~32 and 29 Ma [*Ruffini et al.*, 1995]. Fine-grained synkinematic white micas (2–6 μm) from ductile mylonites at the base of the Morcles and Doldenhorm nappes show staircase $^{40}Ar/^{39}Ar$ age spectra between 13 and 76 Ma [*Kirschner et al.*, 1996]. 94% of the gas release show ages between 13 and 32 Ma that *Kirschner et al.* [1996] interpret as crystallization ages and thus as the duration of the nappe stacking. Such timing

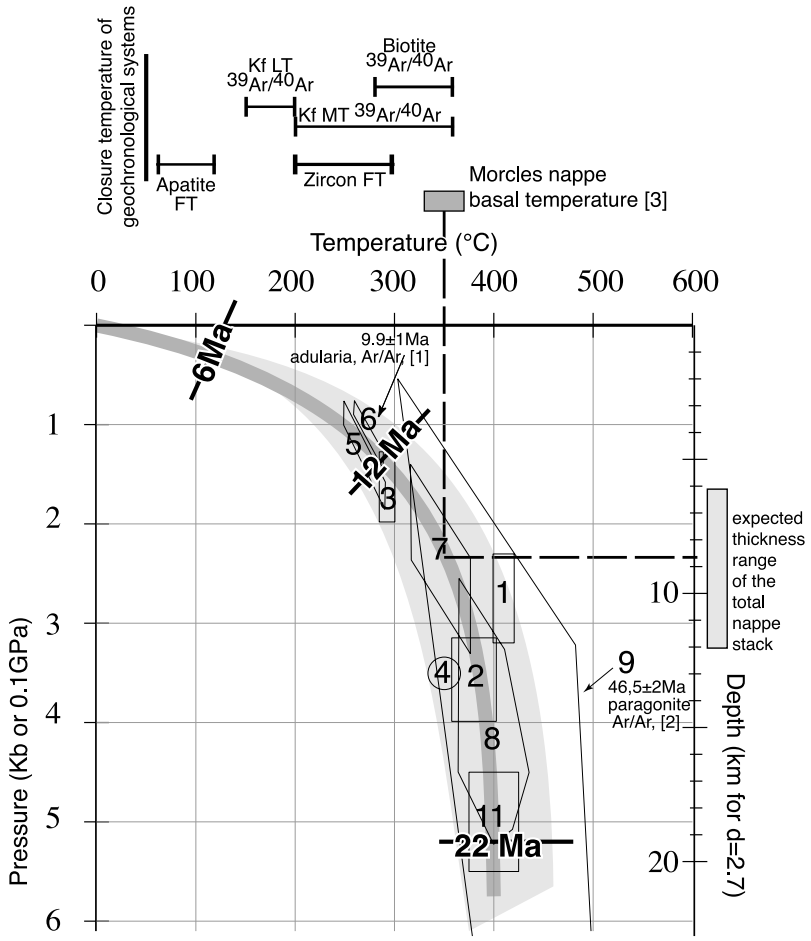

Figure 7. Alpine P-T estimates in the Mont Blanc massif. Labels 1 to 9 are P-T estimates from fluid inclusions in alpine veins: 1 from *Poty et al.* [1974]; 2 (early H_2O-NaCl-rich fluids) and 3 (late H_2O-CO_2 fluids) from *Poty and Cathelineau* [1999]; 4 (Helbronner) from *Fabre et al.* [2002]; 5 (Qtz-Chl veins), 7 (Qtz-Mu veins), 8 (Stilp-Epi-Cc-Qtz veins), and, 9 (Par-Kat Schist), all in the NE part of Mont Blanc, from *Marshall et al.* [1998b]; 6 (Qtz-gold veins, in the NE part of Mont Blanc) from *Marshall et al.* [1998a]; 10 (musc-chlorite equilibria in a musc-biot-chl mylonite within the granite) from *Rolland et al.* [2003]. References are 1, *Marshall et al.* [1998b]; 2, *Marshall et al.* [1998a]; and 3, *Kirschner et al.* [1995]. Nappe thicknesses have been measured from classical cross sections [e.g., *Escher et al.*, 1988]. The data appear to describe the alpine P-T path of the Mont Blanc. Bold ages denote first-order time milestones deduced from geochronological data; see text for discussion.

is confirmed by two independent studies. Small white micas (<2 μm) from a post tectonic vein within the Morcles nappe yield a K/Ar age of ~15 Ma [*Huon et al.*, 1994]. White mica within deformed Mesozoic sediments from the Val Ferret thrust, (~5 km north of Orsières, Figure 2a) yield $^{40}Ar/^{39}Ar$ ages that young toward the fault [*Crespo-Blanc et al.*, 1995]. Of these young ages of 14.6 ± 0.2, 15.5 ± 0.4 and 18.5 ± 0.2, *Crespo-Blanc et al.* [1995] retain the 15.5 Ma age from the thrust surface as indicative of the end of motion.

[27] Apatites fission track ages span from 3.1 to 4.2 Ma in the Aiguilles Rouges, and from 1.4 to 7.5 in the Mont Blanc while most zircon fission track ages span from 11.2 to 15.7 in the Mont Blanc [*Seward and Mancktelow*, 1994; *Soom*, 1990; *Carpéna*, 1992] (Figure 8). According to *Seward and Mancktelow* [1994], age and elevation are not correlated, however most samples were collected along roads or at low altitude with the exception of four samples within the Mont Blanc massif that yield relatively old ages [*Soom*, 1990]. According to *Carpéna* [1992], zircons from the Mont Blanc tunnel and the Aiguille du Midi show a wide fission track age spectra: from 10.8 ± 4.6 to 32.8 ± 0.7 with three age clusters depending on their typology and their U content (Figure 8). Surprisingly, the younger ages are similar to the apatite ages while the older ones are more than 4 Ma older than all other available fission track data (Figure 8). We will thus not consider these two extreme zircon fission track age groups in our interpretation. When plotted together, fission track ages of all ECM (Aar, Belledone, Mont Blanc) show a broad correlation with

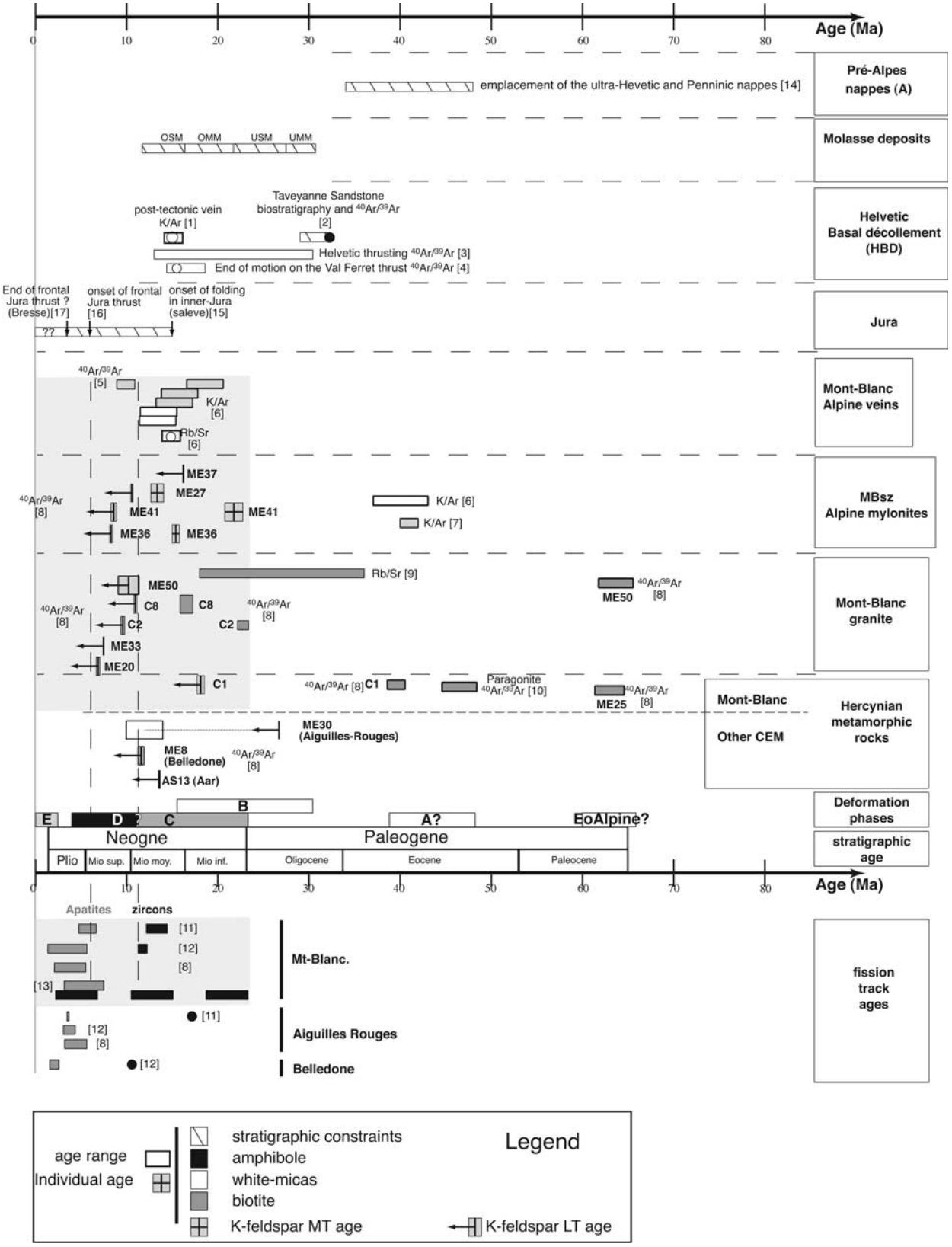
Age (Ma)
0
10
20
30
40
50
60
70
80
Pré-Alpes nappes (A)
emplacement of the ultra-Hevetic and Penninic nappes [14]
Molasse deposits
OSM
OMM
USM
UMM
Helvetic Basal décollement (HBD)
Taveyanne Sandstone biostratigraphy and 40Ar/39Ar [2]
post-tectonic vein K/Ar [1]
Helvetic thrusting 40Ar/39Ar [3]
End of motion on the Val Ferret thrust 40Ar/39Ar [4]
Jura
End of frontal Jura thrust ? (Bresse)[17]
onset of frontal Jura thrust [16]
onset of folding in inner-Jura (saleve)[15]
??
Mont-Blanc Alpine veins
40Ar/39Ar [5]
K/Ar [6]
Rb/Sr [6]
MBsz Alpine mylonites
ME37
ME27
ME41
ME36
K/Ar [6]
K/Ar [7]
Mont-Blanc granite
Rb/Sr [9]
ME50
C8
C2
ME33
ME20
C1
Paragonite 40Ar/39Ar [10]
ME25
Mont-Blanc
Other CEM
Hercynian metamorphic rocks
ME30 (Aiguilles-Rouges)
ME8 (Belledone)
AS13 (Aar)
Deformation phases
E
D
C
B
A?
EoAlpine?
stratigraphic age
Neogne
Paleogene
Plio
Mio sup.
Mio moy.
Mio inf.
Oligocene
Eocene
Paleocene
Apatites
zircons
fission track ages
Mt-Blanc.
Aiguilles Rouges
Belledone
Legend
age range
Individual age
stratigraphic constraints
amphibole
white-micas
biotite
K-feldspar MT age
K-feldspar LT age

Figure 8

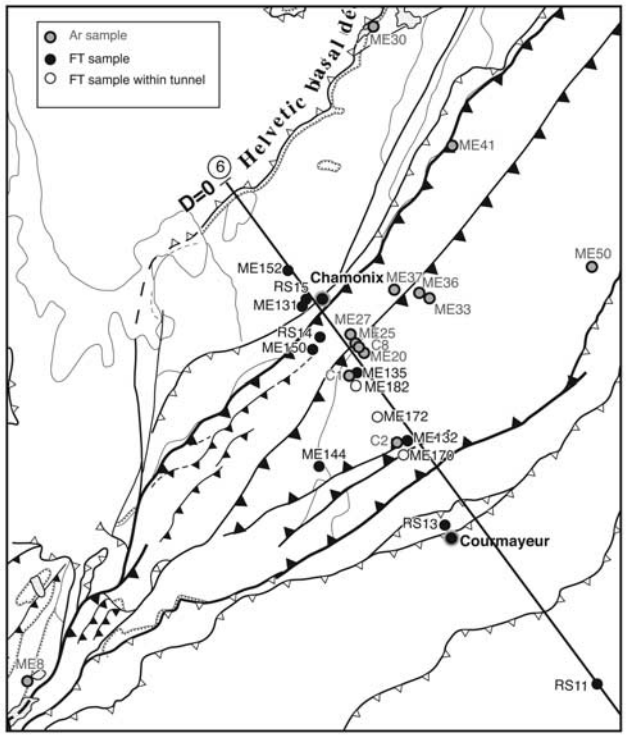

Figure 9. Location of new $^{40}Ar/^{39}Ar$ and fission track data. Location of samples analyzed for fission track and $^{40}Ar/^{39}Ar$ thermochronology. For location, see Figure 2a.

respect to altitude, with a lower slope for zircons than for apatites, an observation that was used to infer an increase of the exhumation rate at ~10 Ma [e.g., *Fügenschuh and Schmid*, 2003].

4.3. New $^{40}Ar/^{39}Ar$ Data

[28] In order to constrain the medium temperature thermal history of the Mont Blanc massif, biotites and K-feldspars from samples of various lithology have been analyzed (Figure 9 and Tables 1a and 1b). Separation and analytic techniques are presented in Appendix A.

4.3.1. Biotites

[29] Biotites from granite samples C2 (Helbroner) and C8 (Plan de l'Aiguille) show good plateau ages at 22.8 ± 0.6 Ma and 22.4 ± 0.1 Ma, respectively, with more than 65% of ^{39}Ar release (Figures 10a and 10b). However, sample C8 has a saddle shape age spectrum, suggesting excess argon. An inverse isochron age of 16.6 ± 0.7 Ma is proposed for this sample (Tables 1a, 1b and Figure 8).

[30] Biotites from samples C1 (granite, Aiguille du Midi) and ME25 (orthogneiss, Plan de l'Aiguille) show good plateaus with more than 85% of total ^{39}Ar released, with ages of 39.2 ± 1.0 Ma and 63.0 ± 1.2 Ma (Figures 10a and 10b). Sample ME50 (granite, La Neuve) shows a disturbed age spectra; a mixed phase obviously degassed during the first heating steps, yielding meaningless old ages. The other steps give a reasonable plateau age of 63.7 ± 2 Ma using 40% of ^{39}Ar released (Figure 10b).

[31] All ages are much younger than the Paleozoic granite emplacement ages, although most of these samples contain minerals that did not experience strong alpine deformation (Tables 1a and 1b). The biotites thus appear to have been reset by at least one alpine thermal event. There are two distinct age groups: around 20 Ma (C2 and C8) and around 63 Ma (ME25 and ME50) (Tables 1a, 1b and Figure 8). C1 yields an intermediate age between the two groups, as do a paragonite sample [*Marshall et al.*, 1998b]. These groups are independent of the location and lithology: C2 and C8 come from opposite flanks of the Mont Blanc, as do ME50 and ME25 (Figure 9).

4.3.2. K-Feldspars

[32] To further constrain the Alpine cooling history, several K-Feldspars have been analyzed (Figure 10, Tables 1a and 1b). Unfortunately, all feldspars from the Mont Blanc massif yield complicated age spectra that prohibit any reasonable thermal modeling.

[33] The initial parts of the age spectra, comprising up to 15% of gas release and corresponding to furnace temperature below 700°C, are the most disturbed, showing alternatively old and young ages (Figures 10c, 10e, and 10g). This is because our heating schedule systematically duplicated the degassing steps; this often results in the second step of every pair having a younger age [cf. *Harrison et al.*, 1994]. In the first part of the age spectra, the ages are correlated with the $^{38}Ar/^{39}Ar$ isotopic ratios (Figures 10d, 10f, and 10h), which can be used as a proxy for the Cl/K ratio. The old ages thus probably correspond to the degassing of Cl-rich inclusions containing excess argon, while the young ages are almost free of excess argon [*Harrison et al.*, 1994].

[34] At around 20% of gas release, most age spectra show a bump in age (Figures 10c, 10e, and 10g). Subsequently, the $^{39}Ar/^{37}Ar$ ratio, proxy for the K/Ca ratio, tends to increase (Figures 10d, 10f, and 10h). This suggests a mineralogical change in the degassing feldspar toward more pure orthoclase. After this bump, some spectra show a small age plateau (Figures 10c and 10g) indicating a medium temperature age (Kf MT average age, Figure 8 and Tables 1a and 1b). Ages corresponding to higher furnace temperatures (1000–1200°C) increase (Kf HT maximum age, Tables 1a and 1b).

Figure 8. Timing constrains on the main Alpine deformations within the Mont Blanc and Aiguilles Rouges massifs. References are 1, *Huon et al.* [1994]; 2, *Ruffini et al.* [1995]; 3, *Kirschner et al.* [1996]; 4, *Crespo-Blanc et al.* [1995]; 5, *Marshall et al.* [1998a]; 6, *Leutwein et al.* [1970]; 7, *Krummenacher and Evernden* [1960]; 8, this study; 9, *Baggio et al.* [1967]; 10, *Marshall et al.* [1998b]; 11, *Soom* [1990]; 12, *Seward and Mancktelow* [1994]; 13, *Carpéna* [1992]; 14, *Pfiffner et al.* [2002]; 15, *Beck et al.* [1998] and *Deville et al.* [1994]; 16, *Becker* [2000]; and 17, *Jan du Chêne* [1974]. The light gray area encompasses the timing of uplift of the Aiguilles Rouges and Mont Blanc massif.

Table 1a. New Argon 40/39 Analyses of Biotites and K-Feldspars From Samples of Various Lithology for the Aar, Belledone, Aiguilles Rouges, and Mont Blanc External Crystalline Massifs

Sample	Location	Altitude, m	Facies	Deformation[a]	Biotite Plateau Age,[b,c] Ma	Biotite Isochrone Age,[b,c] Ma	Kf LT Minimum Age,[b,c] Ma	Kf LT Isochrone,[c] Ma	Kf MT Average,[b,c] Ma	Kf HT Maximum Age, Ma
Aiguilles Rouges										
ME30	Vieux Emosson Lake	2210	gneiss	Variscan			**26.75 ± 0.02**	12 ± 2 (4, 8, 10, 11, 12)		320.00 ± 0.25
Mont Blanc										
C1	Aiguille du Midi	3800	granite	no deformation	**39.6 ± 0.97** (1, 2, 3, 4)	39.4 ± 1.3 (1, 2, 3, 4, 5)	**18.16 ± 0.4**	3.2 ± 1.4 (1 to 6)		56.09 ± 0.15
C2	Pointe Helbroner	3425	granite	no deformation	**22.8 ± 0.6** (1, 2)		**9.62 ± 0.21**	7.7 ± 0.4 (6, 8, 10, 12)		27.65 ± 0.58
ME27	Plan de l'aiguille	2320	gneiss	alpine mylonite (S, N50°, 47°S)			**10.61 ± 0.15**	4.5 ± 0.9 (4, 6, 8, 11–14)	**13.4 ± 0.7** (17–25)	25.12 ± 0.10
ME25	Plan de l'aiguille	2400	othogneiss	Variscan	**63.0 ± 1.6** (1, 2, 3, 4, 5, 6, 7)					
C8	Plan de l'aiguille	2500	granite	no deformation	22.8 ± 0.9 (2, 3)	**16.6 ± 0.7** (2, 3, 4, 5, 6)	**10.98 ± 0.20**	7.8 ± 2.1 (6, 8, 10,12)		26.42 ± 0.15
ME20	Plan de l'aiguille	2620	granite	no deformation			**6.68 ± 0.02**	10.4 ± 4 (1–10)		56.90 ± 0.20
ME37	échelles Montenvers	1820	orthogneiss	alpine mylonite (S, N20°, 65°S)			**16.26 ± 0.01**	11.9 ± 4.1 (1, 2, 4, 6, 8, 12)		110.00 ± 0.40
ME36	échelles Charpoua	2300	granite	moderate deformation (S, N35°, 70°S, alpine?)			**8.35 ± 0.20**		**15.43 ± 0.40** (22–27)	24.30 ± 0.12
ME33	Charpoua	2380	granite	very slight deformation (S, N30°, 90°S, alpine?)			**7.50 ± 0.01**	9.7 ± 1.9 (2, 4, 6, 8, 10, 12, 14, 16, 18, 20)		51.82 ± 0.01
ME41	vallon du Tour	1630	orthogneiss	alpine mylonite (S, N45°, 55°S)			**8.63 ± 0.3**	9.7 ± 0.6 (6, 8, 10, 12)	**21.8 ± 1.0** (23–28)	32.53 ± 0.2
ME50	vallon de l'A Neuve	1960	granite	no deformation	**63.7 ± 1.9** (plateau)		**10.27 ± 1.13**			99.14 ± 0.14
Belledone										
ME8	Gittaz lake	1600	gneiss	Variscan (S, N120°, 55°S)						
Aar										
AS13	north of Wassen		orthogneiss	Alpine foliation (S, N40°, 77°S)			**13.63 ± 0.11**			67.00 ± 0.22

[a]When present, direction of the alpine schistosity (S) appears in parentheses. Alpine? means that we suspect that that deformation is of alpine age (and not Variscan) but we are not sure of this.
[b]For each sample, the retained age appears in bold.
[c]Numbers in parentheses indicate the step numbers on which the ages are based.

Table 1b. New Apatite Fission Tracks Ages for Mont Blanc and Aiguilles Rouges

	Location	Altitude, m	Facies	Deformation	Distance Along Section 6 Figure 9, km	Age, Ma	±1σ
Aiguilles Rouges							
ME 152-1	Brévent summit	2500	gneiss	Variscan	6.3	4.93	0.94
ME131	Les Gaillands	1010	muscovite gneiss	Variscan	8.4	3.78	0.55
Mont Blanc							
ME150	Chalet Cerro	1370	gneiss	Variscan	10.6	3.84	0.3
ME 135	Aiguille du Midi	3800	granite	no deformation	13.65	4.8	0.79
ME 182-2	tunnel (PM = 3850)	1300	granite	very sligth deformation	14.25	4.56	1.03
ME 172 B	tunnel (PM = 6343)	1350	granite	no deformation	16.6	3.35	0.44
ME132	Pointe Helbroner	3425	granite	no deformation	18.35	not countable	
ME170	tunnel (PM = 9242)	1350	granite	no deformation	19.65	2.75	0.52
ME144	Col Major	4760	gneiss	Variscan	16.8	5.04	0.63

[35] Two hypotheses can explain both the general shape of the age spectrum and the corresponding chemical zoning. The first explanation is that degassing of Variscan zoned K-feldspar produced this pattern. The second possibility is that recrystallized rims around inherited Variscan K-rich cores yielded the first and second parts of the age spectrum, respectively. In both hypotheses, the K-feldspar would have been strongly reset during a Cenozoic thermal event, creating the second part of the age spectrum. In the first hypothesis, the initial part of the age spectrum would correspond to the final cooling recorded by the K-feldspar (around 150°C), while in the second hypothesis it would correspond to the age of feldspar recrystallization. We favor that second hypothesis given the widespread occurrence of secondary K-feldspar crystallization in the Alpine veins (adularia) and surrounding rocks of the Mont Blanc massif [e.g., *Rossi et al.*, 2005]. In the Aiguilles Rouges massif, the K-feldspar core was not completely reset and the sample shows a Variscan (≥300 Ma) HT maximum age (ME30, Tables 1a and 1b). On the other hand, in the Mont Blanc massif all feldspars have HT maximum ages less than 110 Ma; eight of the ten samples yield Tertiary ages (Tables 1a and 1b). This indicates that the thermal event reached temperatures close to 400°C, in good agreement with the P-T path (Figure 7). In this context, the medium temperature (MT) plateau ages probably correspond to an episode of rapid cooling. The clearest MT plateaus are found in the alpine mylonites and are between 22 and 13 Ma (Figure 8). We thus suggest that significant cooling from temperatures around 400°C took place in the Mont Blanc massif during this time interval. This would be in good agreement with biotites ages from samples C2 and C8 (Figure 8). Biotite ages are usually considered to reflect cooling below 320 ± 40°C [e.g., *Harrison et al.*, 1978; *Leloup et al.*, 2001].

[36] The age of the feldspar overgrowth (or the last cooling episode) is difficult to calculate precisely due to the presence of excess argon in the first part of the age spectra. Because of this excess argon, the lowest age (Kf LT minimum age, Tables 1a and 1b) is most significant, and is probably the best estimate for the age of the feldspar overgrowth. Sometimes some of the duplicate steps define a low-temperature plateau (Figures 10c, 10e, and 10g). However, these younger steps could also be affected by excess argon, as suggested by inverse isochron ages (Kf LT isochron, Tables 1a and 1b). The Kf LT minimum age is thus considered as a maximum age for the K-feldspar overgrowth (Figure 8). Within the Mont Blanc massif, all K-feldspars have LT minimum ages younger than 18 Ma (Figure 8, Tables 1a and 1b). Of these 10 samples, only two (ME37 and C1) are older than 16 Ma, while all other samples yield ages between 7 and 11 Ma (Figure 8). ME30 from the Aiguilles Rouges yields an older, but still Tertiary, LT age (27 Ma). As stated above, this is a maximum age, and a 12 ± 2 Ma isochron age can be proposed instead (Tables 1a and 1b). Such an age would be in better agreement with the 17 Ma zircon fission track age from the same massif [*Soom*, 1990], as well as Kf LT ages of 12 and 14 Ma obtained in the Belledonne and Aar massifs, respectively (Tables 1a, 1b and Figure 8).

4.4. New Apatite Fission Track Data

[37] In order to constrain the lower part of the cooling history, 8 new apatite fission track ages have been obtained (Figure 11 and Table 2). Most samples lie along a NW-SE section through the Aiguilles Rouges and Mont Blanc massifs, with samples collected between ~1000 m high in the Chamonix valley and the Mont Blanc tunnel and 3800 m on the Aiguille du Midi (section 6, Figures 2a and 9). ME144 is slightly offset from cross section 6, coming from the highest outcrop: above the Col Major at 4760 m of altitude. The fission track methodology is presented in Appendix B.

[38] All ages lie between 2.7 ± 0.5 and 5.0 ± 0.6 Ma (Figure 8 and Tables 1a and 1b), in the same range as previously published ages (Figure 8). Because of the young ages, confined track lengths could not be measured. The highest samples tend to show the oldest ages, but the correlation is difficult to quantify, partly because the uncertainties on the ages are relatively large (Figure 11a, top left).

5. Discussion

[39] The high altitude of outcropping basement rocks in the Mont Blanc and the young apatite fission tracks cooling ages suggest a significant amount of recent rock uplift and

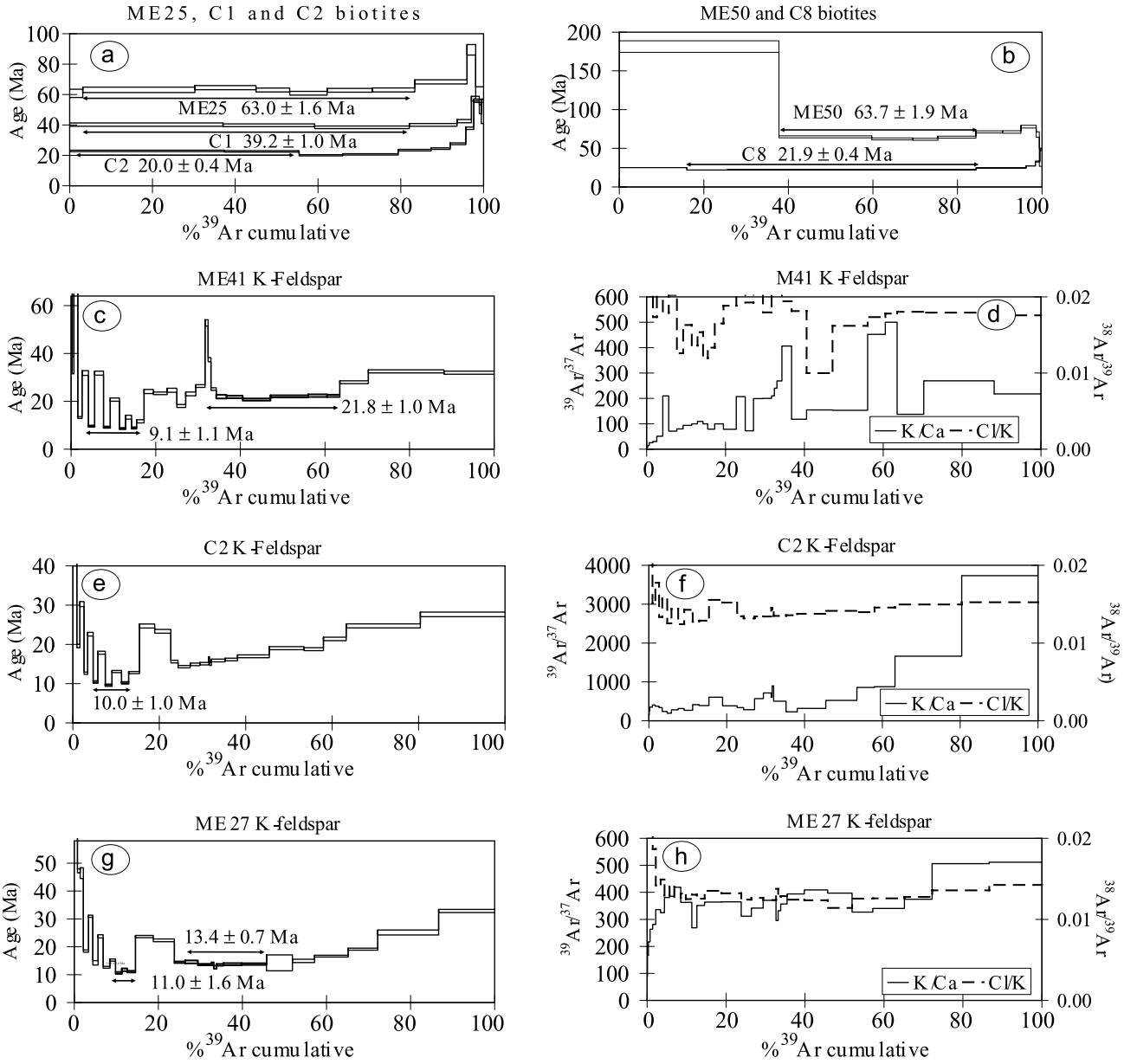

Figure 10. Examples of new $^{40}Ar/^{39}Ar$ data. (a) Biotite age spectra of samples C2, C1, and ME25. (b) Biotite age spectra of samples C8 and ME50. (c, e, g) Kf ages spectra for samples ME41, C2, and ME27. (d, f, h) The $^{38}Ar/^{39}Ar$ (proxy for the Cl/K) and $^{39}Ar/^{37}Ar$ (proxy for the K/Ca) spectra of samples ME41, C2, and ME27, respectively.

exhumation. As will be discussed below, structural studies indicate that uplift occurred by at least three distinct mechanisms: broad doming, reverse/dextral motion along the MBsz and reverse motion along the Mont Blanc back thrust (phases C, D, and E, Figure 2a). As the maximum pressure clearly documented for Alpine times is 5 ± 0.5 kbar (Figure 7), the total amount of exhumation is on the order of 20 km. The vast majority of the medium to low-temperature geochronological data are Neogene in age (Figure 8), indicating that exhumation of the Mont Blanc and Aiguilles Rouges took place during this interval. However, the precise exhumation amounts and timings remain to be deciphered and are discussed below.

5.1. Amount of Motion Along the Chamonix Shear Zone and the Mont Blanc Back Thrust

[40] Prior to final exhumation, the Aiguilles Rouges and the Mont Blanc were overthrust by the package of the Helvetic and PréAlpes nappes along the HBD (B, Figure 2b); most of these nappes have subsequently been eroded away. The total thickness of the nappe package is

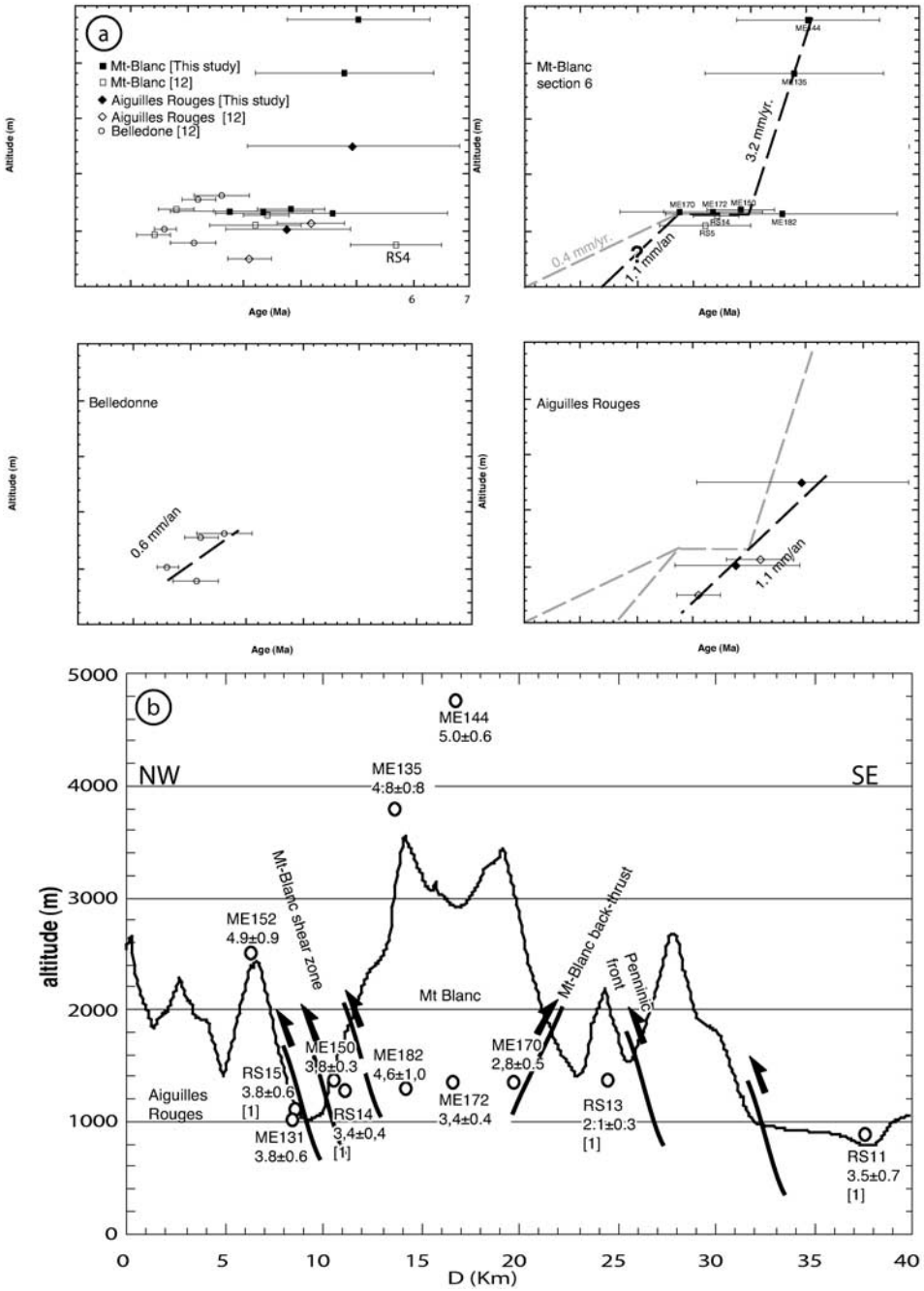

Figure 11. New fission track results. (a) Plot of apatite fission track ages versus altitude. (top left) All ages. (top right) Ages from the Mont Blanc massif along section 6. (bottom left) Ages from the Belledonne massif. (bottom right) Ages from the Aiguilles Rouges massif. Reference 12, from *Seward and Mancktelow* [1994]. RS 4 comes from the NE Mont Blanc near Martigny. For other samples locations, see Figure 9. (b) Cross section of the Mont Blanc massif at the level of the tunnel (6 on Figure 9) with apatite FT sample numbers and ages (see Table 2). Reference 1, from *Seward and Mancktelow* [1994].

estimated to be more than 6 km (thickness of the Morcles nappe alone) and up to 12 km, based on classical cross sections [*Escher et al.*, 1988, 1993; *Pfiffner*, 1993]. Prior to ECM exhumation, the depth and temperature of the Triassic unconformity and the HBD were approximately the same above the Mont Blanc and the Aiguilles Rouges. In the Morcles nappe, temperature estimates from the HBD (350 ± 20°C [*Kirschner et al.*, 1995]) are similar to those suggested by the upper bound of the alpine grade of metamorphism within the Aiguilles

Table 2. Apatite Fission Track Data[a]

Sample	Irradiance	Lithology	Elevation, m	D, km	Nunber of Xls	Rho-S ($\times 10^5$)	NS	Rho-I ($\times 10^5$)	NI	$P(\chi)^2$, %	Rho-D ($\times 10^5$)	ND	Age, Ma	±1σ	U, ppm
ME131	UP38-20	muscovitic gneiss	1010	8.4	22	0.4971	49	169.90	16744	48	69.903	17418	3.8	0.6	30
ME144	UP37-9	gneiss	4760	16.8	21	0.8019	67	37.23	3111	74	12.673	5167	5.0	0.6	37
ME150	UP37-10	dark gneiss	1370	10.6	22	1.3550	181	82.95	11079	95	12.727	5167	3.8	0.3	82
ME170	UP37-12	granite (in tunnel)	1350	19.65	12	0.5093	29	43.89	2499	59	12.835	5167	2.8	0.5	43
ME 135	UP37-8	granite	3800	13.65	24	0.3351	38	16.29	1847	90	12.619	5167	4.8	0.8	16
ME 152-1	UP38-21	gneiss	2500	6.3	25	0.2580	28	68.12	7392	52	70.436	17418	4.9	0.9	12
ME 172 B	UP37-13	granite (in tunnel)	1350	16.6	24	0.5461	60	39.15	4302	26	12.889	5167	3.4	0.4	38
ME 182-2	UP38-23	granite (in tunnel)	1300	14.25	20	0.2699	20	78.10	5787	30	71.503	17418	4.6	1.0	14

[a]Number of Xls is the number of individual crystals dated; Rho-S, Rho-I, and Rho-D are the spontaneous, induced, and dosimetry track density measured (tracks/cm^2); NS and NI are the number of spontaneous and induced tracks counted; $P(\chi)^2$ (%) is the chi-square probability [*Galbraith*, 1981; *Green*, 1981]. Values greater than 5% are considered to pass this test and represent a single population of ages. Rho-D is the induced track density in external detector adjacent to CN5 dosimetry glass (tracks/cm^2); ND is the number of tracks counted in determining Rho-D. Samples analyzed using a zeta of 369.6 ± 7.6 (E. R. Sobel, unpublished data, 2003).

Rouges basement. On Figure 7, such temperatures correspond to 6–12 km depth, in good agreement with the estimated thickness of the nappe package. In the Aiguilles Rouges, the Triassic unconformity now outcrops at 2800 m above sea level (asl) (Aiguille du Belvédère, Figure 2a), corresponding to ~5 km more uplift than 25 km farther NW (Figure 2b). A point now located at the top of the Aiguilles Rouges had thus been buried beneath ~9 ± 3 km of Mesozoic rocks before being uplifted by a total of ~12 ± 3 km (eroded Mesozoic plus present-day altitude) during the Neogene (C, Figure 2b).

[41] The Triassic unconformity is only preserved at the SE and NW extremities of the Mont Blanc and has been completely eroded above the Mont Blanc summit (~4800 m asl) (Figure 2a). This implies a minimum of 2000 m of differential uplift between the Mont Blanc and the Aiguilles Rouges across the MBsz (D, Figure 2b). The observation that the Triassic unconformity describes a broad antiform and must underlie the Mesozoic sediments of the Chamonix valley at ~1000 m asl raises the minimum differential uplift to ~4 km. This value leads to a total exhumation of ~16 ± 3 km for the Mont Blanc rocks, in good agreement with several fluid inclusion P-T estimates (2, 4, 8, Figure 7). The 5 ± 0.5 kbar pressure estimate of *Rolland et al.* [2003] implies an even deeper alpine origin for the Mont Blanc rocks (~20 km) and thus a larger differential uplift (~8 km) across the MBsz (Figure 7).

[42] The amount of exhumation clearly varies both along and across strike of the Mont Blanc. For example, in the NE Mont Blanc, the Triassic unconformity is widely exposed, and exhumation has been limited to the thickness of the overlying nappes (9 ± 3 km). The unconformity dips 60° to 70° to the east. Assuming that the unconformity was initially horizontal and that the 8 to 14 km wide massif was rigidly tilted leads to 7–13 km more uplift along the western flank of the massif than along the eastern one, and thus to a total exhumation of 13–25 km in the west. This is in good agreement with the pressure estimates from *Rolland et al.*'s [2003].

[43] Along strike the level of erosion is clearly shallower SW and NE of the Mont Blanc, where the Helvetic nappes are preserved. Furthermore, the deepest erosion levels correspond to the highest elevations. This implies an important spatial variation in the total exhumation. A straightforward interpretation is that the throw on the MBsz dies out SW and NE of the Mont Blanc with maximum offsets between Chamonix and l'Argentiere. One may note that in the footwall of the MBsz, exhumation variations in the Aiguilles Rouges mimics but are smaller than in the Mont Blanc.

[44] A more detailed look at the topography highlight another mechanism. Elevation decreases abruptly SW of the summit of the Mont Blanc and more gradually toward the NE. Elevations exceeding 4000 m are located almost exclusively in the hanging wall of the Mont Blanc back thrust, from the Grandes Jorasses to the Mont Blanc itself. The latter is located where the Mont Blanc back thrust meets the MBsz (Figure 2a) suggesting that the highest altitudes result from the interaction of these two structures. We suggest that altitudes reached a maximum of 4000 m in the hanging wall of the MBsz (Aiguille Verte), while the exceptional altitude of the Mont Blanc is due to further motion on the Mont Blanc back thrust (E, Figure 2b) that added ~1 km of uplift.

5.2. Timing of Deformation Phases

[45] Until now, timing of exhumation of the ECM has been exclusively discussed on the light of fission track data [e.g., *Seward and Mancktelow*, 1994]. Our new geochronologic data provides a broader perspective for establishing the absolute timing of the tectonic phases discussed in section 3.6. With the exception of U/Pb ages that correspond to the timing of Variscan deformation and granite emplacement (~300 Ma), all of our data are Tertiary in age, mostly distributed between 22 and 2 Ma. Only six analyses yield much older ages between 40 and 64 Ma (Figure 8). Structural relationships imply that uplift and exhumation of the Aiguilles Rouges and Mont Blanc postdates most of the

motion on the HBD, which ended around 15 Ma [*Huon et al.*, 1994; *Kirschner et al.*, 1996; *Crespo-Blanc et al.*, 1995] (Figure 8). The simplest interpretation is thus that most of the rock uplift of the Mont Blanc took place since 22–15 Ma, while older ages likely correspond to previous thermal or tectonic events.

5.2.1. Neogene Exhumation of the External Crystalline Massifs

[46] Because of the complexity of $^{40}Ar/^{39}Ar$ K-feldspar spectra and the relative spread of the other argon and Rb/Sr ages between 22 and 9 Ma, detailed interpretation of the geochronological data is not straightforward.

[47] We interpret the biotite minimum Rb/Sr ages, the zircon fission track ages and some of the $^{40}Ar/^{39}Ar$ ages (C2 and C8 biotites, ME41, ME27, and ME36 Kf MT average age) as reflecting cooling of the Mont Blanc between $\geq$400 and $\sim$300°C, between 22 and $\sim$12 Ma. For biotites, the closure temperature is estimated at 320 ± 40°C for the argon system, and 300 to 350°C for the Rb/Sr system [e.g., *Harrison et al.*, 1978]. Such temperatures are compatible with the K-feldspar argon closure temperature, as well as high values for zircon fission track closure temperatures (250 ± 50°C [*Hurford*, 1986]). This cooling would be concomitant with the crystallization of muscovite and K-feldspar in the alpine veins (18.3–13.4 K/Ar and Rb/Sr ages, Figure 8). Compared with the Mont Blanc average P-T path, such cooling would correspond to 8 to 14 km of exhumation depending on the pressure estimate considered as a starting point for the uplift history (2 or 11, Figure 7).

[48] The young $^{40}Ar/^{39}Ar$ ages (Kf-LT minimum ages) are mostly between 11 and 6 Ma. These are interpreted as the age of feldspars overgrowths (see above), which probably formed around 150–200°C. The $^{40}Ar/^{39}Ar$ age of adularia crystallization in the most superficial alpine veins is within this age range (Figures 7 and 8). That time interval could correspond to $\sim$5 km of exhumation of the Mont Blanc (Figure 7).

[49] The few zircon fission track and K-feldspar LT data from the Aiguilles Rouges are older than those from the Mont Blanc. According to these data, the Aiguilles Rouges cooled below 300°C around 17 Ma, $\sim$4 Myr prior to Mont Blanc (Figure 8). Cooling below 150–200°C occurred at $\sim$12 Ma, synchronously with the Belledonne massif but 1 to 4 Myr prior to the Mont Blanc (Figure 8).

[50] All apatite FT ages are younger than 7.5 Ma (Table 2 and Figures 8 and 11a, top right). The apatite crystals have cooled from temperatures above their total annealing temperature ($\leq$150°C [*Ketcham et al.*, 1999]) and record information on their cooling path during exhumation [e.g., *Green et al.*, 1989a, 1989b]. However, for such young apatites, it is difficult to obtain sufficient track length measurements to permit robust thermal modeling. Given the evidence of rapid cooling, the data are thus simply taken to indicate the time at which the samples passed through the partial annealing zone ($\sim$150–60°C). Given the young ages and their average uncertainty, typically $\sim$0.5 Ma, precise calculation of exhumation rates is impossible. However, first-order observations can be made.

[51] 1. Along section 6, apatite fission track ages on both sides of the Mont Blanc shear zone at altitude below 1500 m are $\sim$4 Ma (Figure 11b). Thus it appears that there has been no significant differential unroofing between the two massifs since that time.

[52] 2. On the other hand, $\sim$5 Ma samples are located $\sim$2000 m higher on the Mont Blanc than on the Aiguilles Rouges (Figure 11b).

[53] 3. On a plot of age versus altitude, a correlation can tentatively be proposed with three distinct trends (Figure 11a, top right): an exhumation rate of a few millimeters per year before $\sim$4 Ma, then a $\sim$1.5 Myr period of slow exhumation, followed by a final pulse of rapid exhumation during the last $\sim$2–3 Myr. This last phase of rapid cooling is inferred from the very young ages of some apatite ($\sim$2.5 Ma) implying an exhumation rate that cannot be lower than 0.4 mm/yr (Figure 11a, top right) and is more probably $\sim$1 mm/yr, as in the Aiguilles Rouges (Figure 11a, bottom right).

[54] 4. Along section 6, within the Mont Blanc, the low-altitude samples, mostly within the tunnel, tend to give younger ages toward the SE (Figure 11b). This suggests more recent exhumation on the SE flank of the Mont Blanc, probably along the back thrust. However, no jump in age is detectable across that structure, probably because of the very young age of the samples (Figure 11b).

[55] 5. Along strike, younger apatite fission track ages ($\sim$1.5 Ma) are observed at the NE end of the Mont Blanc [*Seward and Mancktelow*, 1994]. This may reflect lateral growth of the back thrust towards the NE, where it is not yet clearly expressed.

[56] The data discussed above allow us to propose first-order absolute time milestones along the global P-T path followed by the Mont Blanc rocks (Figure 7). However, given the uncertainty in age, temperature, and pressure, it is difficult to determine whether the exhumation rate, 0.8 ± 2 mm/yr averaged over the last 22 Myr, actually varied significantly during this time. For example, following the global Mont Blanc P-T curve, one can propose that between 22 and 12 Ma the cooling rate was 11°C/Myr, corresponding to an exhumation rate of $\sim$1.4 mm/yr, while from $\sim$12 to $\sim$6 Ma the cooling rate increased to 28°C/Myr but corresponds to a lower exhumation rate of 0.8 mm/yr. However, such figures have large uncertainties and rest on a global P-T path that does not take sample location, advection or topographic affects into account.

5.2.2. Pre-Neogene Geochronological Data

[57] Data older than 40 Ma have to be interpreted with caution. The oldest $^{40}Ar/^{39}Ar$ biotite data (C1, ME25, and ME50), the paragonite $^{40}Ar/^{39}Ar$ data [*Marshall et al.*, 1998a], the $\sim$40 Ma mica K/Ar ages, as well as the oldest biotite Rb/Sr ages [*Baggio et al.*, 1967] (Figure 8), could be ascribed to a partial resetting of Variscan ages leading to spurious intermediate ages. However, in the case of the $^{40}Ar/^{39}Ar$ biotite ages, 1 Myr at $\sim$400°C should be sufficient to completely reset the K/Ar isotopic system, and partial resetting should have produced less

regular age spectra. Unfortunately, inverse isochron plots for these samples are either unpublished or meaningless. The only exception is C1, which yields a 39.4 ± 1.3 Ma isochron age very close from the plateau age (Tables 1a and 1b). Thus the existence of early tectono-thermal events around 63 Ma (ME25 and ME50) and between 40 and 50 Ma (C1, paragonite, and K/Ar ages) cannot be totally excluded. Ages around 40 Ma could reflect Eocene underthrusting of the Mont Blanc below the Penninic basal thrust, in accordance with stratigraphic constraints for the age of the Ultra Helvetic and Penninic nappes [e.g., *Pfiffner et al.*, 2002] (A, Figures 2b, 8, 12a, and 12b). The geological interpretation of the 63 Ma data is more obscure. It is difficult to understand what event could have reset ME25 and ME50 biotites within the Mont Blanc located far to the west from the deformation front at ~63 Ma (see Figure 12a).

5.2.3. Proposed Alpine P-T-t-D History of the Mont Blanc Massif

[58] Taking the previous discussion into account, we propose the following scenario for the Alpine structural evolution of the Mont Blanc and Aiguilles Rouges (Figure 12).

[59] 1. In the early Eocene, prior to alpine deformation, the Mont Blanc and Aiguilles Rouges were buried below the subalpine (Helvetic) sedimentary series (Figure 12a).

[60] 2. During the upper Eocene, the Versoyen and Valaisan series were thrust to the north along the Penninic décollement (phase A, Figures 2a, 8, and 12b).

[61] 3. Between ~30 and ~15 Ma, thrusting took place along the HBD, bringing the Helvetic (subalpine) nappes on top of the future ECM. At that time, deeper parts of the Mont Blanc reached ~400°C and 14–20 km depth, while the upper part of the Aiguilles Rouges was at ~9 km depth and ~300°C (phase B, Figures 2a, 8, 12c, and 12d).

[62] 4. Around 22 Ma, initiation of the alpine sole thrust induced uplift of the ECM with doming of the Aiguilles Rouges and tilting of the Mont Blanc (phase C, Figures 2a, 8, and 12d).

[63] 5. At ~12 Ma, movement on the MBsz induced relative vertical motion between the Aiguilles Rouges and Mont Blanc. Uplift slowed down in the Aiguilles Rouges while it remained rapid in the Mont Blanc, leading to 4 to 8 km of additional uplift (phase D, Figures 2a, 8, 12e, and 12f).

[64] 6. Prior to ~4 Ma, motion on the MBsz shear zone stopped; subsequent exhumation results primarily from activation of the Mont Blanc back thrust, leading to the final elevation of the southern part of the Mont Blanc massif (phase E, Figures 2a, 8, and 12g). Apatite F-T data suggests that the Mont Blanc back thrust could have initiated at ~2.5 Ma.

5.3. Implications for the Structural Evolution of the Alps

[65] Northwest of the Mont Blanc, the Jura is an arcuate fold belt created by thin-skinned tectonics above a décollement level in the Triassic evaporites (Figure 1). NW of the Mont Blanc, the Jura folds account for 20 to 28 km shortening in a NW-SE direction [*Guellec et al.*, 1990; *Affolter and Gratier*, 2004]. The Jura décollement can either root below the Aiguilles Rouges or be continuous with the HBD and root farther to the SE. A key point to distinguish between these two hypotheses is the timing of ECM uplift [e.g., *Affolter*, 2003]. Deformations in the inner Jura started around 15 Ma [*Beck et al.*, 1998; *Deville et al.*, 1994] and propagated to the external Jura at 6 ± 3 Ma [*Becker*, 2000]. Folding above the Jura décollement thus started when motion on the HBD stopped, at a time of important uplift in the ECM (Figures 8, 12d, and 12e). This strongly suggests that the Jura décollement does not root within the HBD, but rather that the ECM uplift was linked to the transfer of motion from the HBD to a deeper and more external thrust system: the alpine sole thrust (Figure 12). The existence of such a thrust has been proposed by several authors [e.g., *Ménard and Thouvenot*, 1987; *Butler*, 1985; *Lacassin et al.*, 1990] as the most probable cause for uplift of the Aiguilles Rouges and the Belledonne massif. Some SE dipping reflectors along the ECORS seismic line (C on Figure 12h) could correspond to the trace of such thrust. However, the ECM are never clearly thrust above the subalpine sediments [e.g., *Gidon*, 2001]. Our interpretation is that the basal thrust merged with the preexistent HBD before propagating farther west below the Jura (Figures 12d and 12e). The ECM are thus thrust upon the basement rather than the Mesozoic sediments (Figure 2b), and form a backstop whose 20 to 28 km motion toward the NW since ~22 Ma induced the arcuate structure of the Jura.

[66] Our study appears to confirm three successive stages (Penninic, Helvetic, Jura) of deformation, implying a ~100 km long flat décollement in the external part of the orogen while deformation rooted in the more internal part

Figure 12. Structural evolution of the external Alps. (a–g) Structural evolution of the external Alps along a NW-SE section across the Aiguilles Rouges and Mont Blanc massifs, depicted seven time steps from 50 Ma to present-day. Note that the structural evolution of the internal Alps, mostly occurring before 32 Ma, is not depicted. Shortening estimates in the Jura and Helvetic nappes from *Affolter* [2003]. A to D refer to the main deformation phases in the Aiguilles Rouges and Mont Blanc massifs (see also Figures 2b and 8). Note that the bottom line of the section does not correspond to the Moho but rather to a passive marker at the top of the layered lower crust. (h) ECORS-CROP seismic line for broad comparison with Figure 12g [from *Schmid and Kissling*, 2000]. Some structures, such as the Mont Blanc back thrust, are offset from this seismic line, which goes through Belledonne south of the Mont Blanc (see Figure 1a). See color version of this figure at back of this issue.

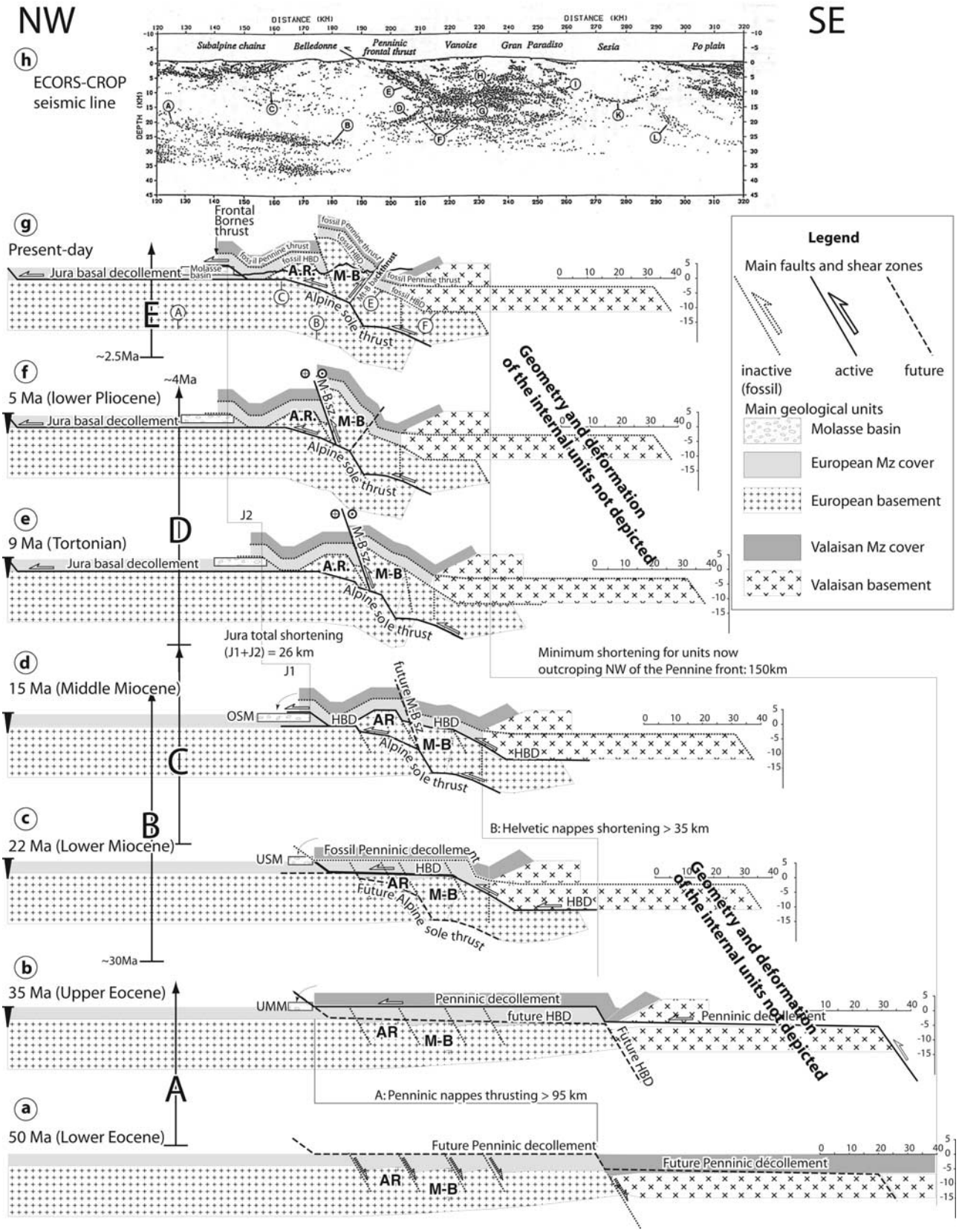
NW
SE
h
ECORS-CROP seismic line
DISTANCE (KM)
DEPTH (KM)
Subalpine chains
Belledonne
Penninic frontal thrust
Vanoise
Gran Paradiso
Sesia
Po plain
g
Present-day
Frontal Bornes thrust
Jura basal decollement
Molasse basin
A.R.
M-B
Alpine sole thrust
~2.5Ma
f
5 Ma (lower Pliocene)
~4Ma
M-B sz
e
9 Ma (Tortonian)
J2
d
15 Ma (Middle Miocene)
J1
OSM
HBD
AR
future M-B sz
c
22 Ma (Lower Miocene)
USM
Fossil Penninic decollement
Future Alpine sole thrust
~30Ma
b
35 Ma (Upper Eocene)
UMM
Penninic decollement
future HBD
a
50 Ma (Lower Eocene)
Future Penninic decollement
Future Penninic décollement
Jura total shortening (J1+J2) = 26 km
Minimum shortening for units now outcroping NW of the Pennine front: 150km
B: Helvetic nappes shortening > 35 km
A: Penninic nappes thrusting > 95 km
Geometry and deformation of the internal units not depicted
Legend
Main faults and shear zones
inactive (fossil)
active
future
Main geological units
Molasse basin
European Mz cover
European basement
Valaisan Mz cover
Valaisan basement

Figure 12

(Figure 12). Each décollement phase was active for 15 to 20 Myr and progressively stepped toward the foreland. This simple scenario of externally vergent propagation was complicated by the ~12 Ma activation of the steep MBsz, which acted as an out of sequence thrust. While finite shortening above the Jura decollement strikes NW [*Affolter and Gratier*, 2004], perpendicular to the trend of the MBsz, that shear zone has a small dextral component. The geometry of the shear zone imply that 4 km of vertical uplift of the Mont Blanc would correspond to 5.5 km of throw on the fault, with 5.4 and 1 km of downdip and right-lateral motion, respectively. This corresponds to 3.7 km of horizontal shortening in the N110 direction. An 8 km vertical motion would correspond to 2.1 km of right-lateral motion for 7.5 km of shortening. The component of right-lateral shear might explain the few NE-SW dextral brittle faults observed (Figure 6). Neogene NE-SW dextral faulting in the Mont Blanc was first proposed by *Gourlay* [1983]. *Hubbard and Mancktelow* [1992] later suggested an offset of 15 km, on a fault zone running along the Mont Blanc massif and connecting the Simplon normal shear zone to the Pelvoux (Figure 1). However, exposures of the corresponding structures are scarce, and the proposed offset disputable. If motion on the MBsz is indeed compatible with a NE-SW right-lateral transpressive regime, it accounts for less than a couple of kilometers of dextral motion between ~12 and ~4 Ma. Alternatively, right-lateral shear could have taken place after the end of motion on the MBsz ~4 Ma. Indeed, farther SW earthquake location and focal mechanisms suggest that the outer Belledonne massif (Figure 1) is followed by a right-lateral seismic fault that could merge with the Chamonix Valley [*Thouvenot et al.*, 2003]. However, the strike of such fault is barely compatible with that of the Mont Blanc back thrust (see section 3.6). It follows that either the prolongation of the active Belledone fault is not along the Mont Blanc; or that the Mont Blanc back thrust is now inactive. Given the very high altitude of the Mont Blanc and the impressive morphology of its southern flank we favor the first hypothesis.

[67] As the Aiguilles Rouges and the Mont Blanc massifs are separated by the Chamonix syncline, the other ECM are split along strike by a narrow band of Mesozoic rocks: the synclinal median between the internal and external Belledonne, and the Furka-Andermatt synclinorium between the Gothar and Aar massifs (Figure 1). In the Belledonne the synclinal median has been interpreted as the trace of right-lateral strike-slip faulting in the prolongation of the Chamonix synclinorium but with very little field evidence [e.g., *Gourlay*, 1983; *Hubbard and Mancktelow*, 1992]. In the Aar the synclinorium has been interpreted as the root of one of the Helvetic nappes [e.g., *Escher et al.*, 1988]. While alpine deformation is probably more distributed in Belledone and in Aar than in the Mont Blanc [e.g., *Choukroune and Gapais*, 1983], it is very tempting to interpret these other Mesozoic synclinoriums as footwalls of steep faults similar to the MBsz. This would imply that a large breach fault with a minor dextral component affected the ECM from Aar to Belledone during the Neogene. However, this hypothesis needs to be tested by further structural and geochronologic studies.

[68] The very high altitude of the Mont Blanc appears to result from the interaction of two steep thrust faults, one of may still be active today (Figure 12g). While most of the subalpine anticlines in the hanging wall of the HBD are strongly eroded, in good agreement with the end of motion along that fault at ~15 Ma, the most external of these folds have a juvenile, whale-back morphology. This suggests either a very young age or a recent reactivation of the Bauges frontal thrust (Figure 12g). Such observations strongly suggest that the alpine sole thrust is still active today and that shortening is still taking place north of the Penninic front. The same conclusion is reached when looking at seismologic studies (see synthesis of *Sue and Tricart* [2003, chapter 5.2]). On the other hand, south and east of the Penninic front, some structural and seismologic data suggest radial extension [e.g., *Sue and Tricart*, 2003], and GPS measurements tend to indicate a net extension across the Alps [*Calais et al.*, 2002; *Vigny et al.*, 2002]. Determining the period that compression in the external part of the orogen has been coeval with extension in the internal part, and understanding the mechanism for this style of deformation remains a major question for the study of continental lithosphere mechanics during collision.

Appendix A: The $^{40}Ar/^{39}Ar$ Techniques

[69] High purity aliquots in the range 180–250 μm were separated using heavy liquids, magnetic separation, and handpicking. Separates were irradiated at Ford Nuclear Reactor of the University of Michigan in the L67 position for 28 hours for samples C1, C2 and C8, and 50 hours for all other samples. The J factor was estimated by analyzing duplicates of the Fish Canyon sanidine standard (28.02 Myr [*Renne et al.*, 1998]), irradiated between every 10 samples, yielding a 1% relative standard deviation. CaF_2 and K_2SO_4 salts were used to account for interfering nuclear reactions. Step heating analysis were performed at the $^{40}Ar/^{39}Ar$ laboratory in Clermont-Ferrand on a VG3600 mass spectrometer in a way similar to that described by *Arnaud et al.* [2003]. Average blanks for ^{40}Ar range from 1.3×10^{-15} mol STP at low temperature to 4.7×10^{-15} mol STP at 1200°C on both furnaces and have been reproducible over the years. Blanks for other masses are usually under detection level or so low that they have large uncertainties. Age spectrum calculations are given at 1σ on each step and include all correction factors, as well as 2% errors on blanks taken for correction. Individual steps do not include error on J factor, while plateau and isochron ages do, with an average of 1.5%. Comparison of several isotopes allows qualitative analysis of K/Ca ($^{39}Ar/^{37}Ar$) and Cl/K ($^{38}Ar/^{39}Ar$) ratios. Note that for simplicity, K/Ca and Cl/K will be used in the text while no strict calculations have been made and those terms only reflect the isotope ratios. Results are shown in Tables 1a and 1b. Plateau ages and isochrons are calculated following the criteria of *Dalrymple et al.* [1981] and *Roddick et al.* [1980].

[70] A particularly long furnace heating schedule was conducted on K-feldspar in order to try to retrieve diffusion

characteristics, to apply diffusion models, and to calculate model thermal histories [e.g., *Lovera et al.*, 1991].We also conducted two-stage isothermal stepwise heating at low temperatures (450–800°C); the first and the second of the two isothermal stages lasting of the order of 10 and 15 min, respectively. Such a heating schedule often produces a saw tooth-shaped age spectrum where the second of the two stages is systematically younger and less affected by excess argon [e.g., *Harrison et al.*, 1994].

[71] We have assumed closure temperatures of 320 ± 40°C for biotites [e.g., *Harrison et al.*, 1978; *Leloup et al.*, 2001]. For K-feldspars, the calculation of a cooling history using diffusion models was impossible. We qualitatively considered that the lower furnace temperature (LT, 400–700°C) ages correspond to cooling at ~150–300°C, whereas higher furnace temperatures (HT, 1000–1200°C) ages correspond to cooling at ~300–450°C [e.g., *Leloup et al.*, 2001].

Appendix B: Fission Track Methodology

[72] Apatite was separated using standard magnetic and density methods, then mounted on glass slides with araldite epoxy. After grinding and polishing to expose an internal surface, the apatites were etched with 5.5 molar nitric acid for 20 s at 21°C. Samples were irradiated in two groups at Oregon State University; one of the groups had 5 times the dose of the other. After irradiation, mica external detectors were etched in 40% HF for 45 min at 21°C. For age determinations, 12 to 25 good quality grains per sample were selected at random and dated using the external detector method. Laboratory procedures are essentially the same as reported by *Sobel and Strecker* [2003]. Additional analytical details are presented in Table 2. Following convention, all statistical uncertainties on pooled ages and mean track lengths are quoted at the ±1σ level, but ±2σ uncertainties are taken into account for geologic interpretation.

[73] **Acknowledgments.** We acknowledge Marc Poigniez and A. Vigna for helping us to access under ground samples from within the Mont Blanc tunnel. Chamonix Mont Blanc Helicoptères allows us to gather large samples from high altitudes. This sampling would not have been possible without the help of the PGHM nor the kindness of the Aiguilles Rouges and StGervais natural reserves as well as the Chamonix and StGervais communes. F. Masson and the Montpellier geophysical team are thanked for their help in the field. This project was founded by a CNRS ATI grant to P.H.L. and N.A. and by the INSU/BRGM geofrance 3D program. Enthusiastic (J. M. Lardeaux) and skeptical (O. A. Pfiffner) reviews improved the final manuscript.

References

Affolter, T. (2003), Etude des d'formations et restauration 3D d'un basin de front de chaîne: L'exemple du Jura et des massifs subalpins français, Joseph Fourier thesis, Joseph Fourier Univ., Grenoble, France.

Affolter, T., and J. Gratier (2004), Map view retrodeformation of an arcuate fold-and-thrust belt: The Jura case, *J. Geophys. Res.*, *109*, B03404, doi:10.1029/2002JB002270.

Antoine, P., J. L. Pairis, and B. Pairis (1975), Quelques observations nouvelles sur la structure de la couverture sédimentaire interne du massif du Mont-Blanc, entre col Ferret (frontière italo-suisse) et la tête des fours (Savoie, France), *Géol. Alpine*, *51*, 5–23.

Antoine, P., et al. (1979), Geological map of France, scale 1/50,000, sheet Mont-Blanc (704), Bur. de Rech. Geol. et Min., Orléans, France.

Aprahamian, J. (1988), Cartographie du métamorphisme faible à très faible dans les Alpes françaises externe par l'utilisation de la cristallinité de l'illite, *Geodin. Acta*, *2*, 25–32.

Arnaud, N., P. Tapponnier, F. Roger, M. Brunel, U. Scharer, C. Wen, and X. Zhiqin (2003), Evidence for Mesozoic shear along the western Kunlun and Altyn-Tagh fault, northern Tibet (China), *J. Geophys. Res.*, *108*(B1), 2053, doi:10.1029/2001JB000904.

Ayrton, S. (1969), Déformations des séries autochtone et Helvétique au SE du massif du Mont-Blanc, *Eclogae Geol. Helv.*, *62*, 95–104.

Ayrton, S. (1980), La géologie de la zone Martigny-Chamonix (versant Suisse) et l'origine de la nappe de Morcles (un exemple de subduction continentale), *Eclogae Geol. Helv.*, *73*, 137–172.

Baggio, P. (1964), Contributo alla conoscenza geologica del versante italiano del Monte Bianco, *Atti Ist. Veneto Sci.*, *122*, 293–325.

Baggio, P., G. Ferrara, and R. Malaroda (1967), Results of some Rb/Sr age determinations of the rocks of the Mont Blanc tunnel, *Boll. Soc. Geol. Ital.*, *86*, 193–212.

Beck, C., E. Deville, E. Blanc, Y. Philippe, and M. Tardy (1998), Horizontal shortening control of the middle Miocene marine siliciclastic accumulation (Upper Marine Molasse) in the southern termination of the Savoy Molasse Bassin (northwestern Alps/southern Jura), in *Cenozoic Foreland Basins of Western Europe*, edited by M. Fernandez, *Geol. Soc. Spec. Publ.*, *134*, 263–278.

Becker, A. (2000), The Jura mountains: An active foreland fold-and-thrust belt?, *Tectonophysics*, *321*, 381–406.

Bellière, J. (1956), Caractère de la déformation Alpine dans les schistes cristallins du massif du Mont-Blanc, *Bull. Soc. Geol. Fr.*, *VI*, 691–698.

Bellière, J. (1988), On the age of mylonites within the Mont-Blanc massif, *Geodin. Acta*, *2*, 13–16.

Bellière, J., et al. (1987), Geological map of France, scale 1/50,000, sheet Chamonix (680), Bur. de Rech. Geol. et Min., Orléans, France.

Bertini, G., M. Marcucci, R. Nevini, P. Passerini, and G. Sguazzoni (1985), Patterns of faulting in the Mt Blanc granite, *Tectonophysics*, *11*, 65–106.

Bonin, B., et al. (1993), Late Variscan magmatic evolution of the alpine basement, in *Pre-Mesozoic Geology in the Alps*, edited by J. F. Von Raumer and F. Neubauer, pp 171–201, Springer, New York.

Bussy, F. (1990), Pétrogénèse des enclaves microgrenues associées aux granitoïdes calc-alcalins: Example des massifs varisque du Mt-Blanc (Alpes occidentales) et Miocène du Monte Capanne (Ile d'Elbe, Italie), Ph.D. thesis, Univ. of Lausanne, Lausanne, Switzerland.

Bussy, F., and J. F. Von Raumer (1993), U-Pb dating of Palaezoic events in the Mont-Blanc crystalline massif, western Alps, *Terra Nova Abstr.*, *5*, 382.

Bussy, F., U. Schaeltegger, and C. Marro (1989), The age of the Mont-Blanc granite (western Alps): A heterogeneous isotopic system dated by Rb-Sr whole rock determinations on its microgranular enclacves, *Schweiz. Mineral. Petrogr. Mitt.*, *69*, 3–13.

Bussy, F., J. Hernandez, and J. F. Von Raumer (2001), Bimodal magmatism as a consequence of the post-collisional readjustment of the thickened Variscan continental lithosphere (Aiguilles Rouges-Mont-Blanc massifs, western Alps), *Spec. Pap. Geol. Soc. Am.*, *350*, 221–233.

Butler, R. (1983), Balanced cross-sections and their implications for deep structure of the northwest Alps, *J. Struct. Geol.*, *5*, 125–138.

Butler, R. (1985), The restoration of thrust systems and displacement continuity around the Mont-Blanc massif, NW external Alpine thrust belt, *J. Struct. Geol.*, *7*, 569–582.

Calais, E., J. M. Nocquet, F. Jouanne, and M. Tardy (2002), Current strain regime in the western Alps from continuous Global Positioning System measurements 1996–2001, *Geology*, *30*, 651–654.

Capuzzo, N., and F. Bussy (1999), Volcanic input in a late Paleozoic tectono-sedimentary basin: The Salvan-Dorénaz basin (south-western Switzerland–Eastern France), *Terra Abstr. Abstr.*, *11*, 297.

Capuzzo, N., R. Handler, F. Neubauer, and A. Wetzel (2003), Post-collisional rapid exhumation and erosion during continental sedimentation: The example of the late Variscan Salvan-Dorénaz basin (Western Alps), *Int. J. Earth Sci.*, *92*, 364–379.

Carpéna, J. (1992), Fission-track dating of zircons: Zircons from Mont Blanc granite (French-Italian Alps), *J. Geol.*, *100*, 411–421.

Choukroune, P., and D. Gapais (1983), Strain pattern in the Aar granite (central Alps): Orthogneiss developed by bulk inhomogeneous flattening, *J. Struct. Geol.*, *5*, 1–10.

Crespo-Blanc, A., H. Masson, Z. Sharp, M. Cosca, and J. Hunziker (1995), A stable and $^{40}Ar/^{39}Ar$ isotope study of a major thrust in the Helvetic nappes (Swiss Alps): Evidence for fluid flow and constraints on the nappe kinematics, *Geol. Soc. Am. Bull.*, *107*, 1129–1144.

Dalrymple, G. B., E. C. Alexander Jr., M. A. Lanphere, and G. P. Kraker (1981), Irradiation of samples for $^{40}Ar/^{39}Ar$ dating using the Geological Survey TRIGA reactor, *U.S. Geol. Surv. Prof. Pap.*, *1176*, 55 pp.

Deville, E., E. Blanc, M. Tardy, C. Beck, M. Cousin, and G. Ménard (1994), Thrust propagation and syntectonic sedimentation in the Savoy Tertiary Molasse Basin (Alpine foreland), in *Hydrocarbon and petroleum geology of France*, *Spec. Publ.*

Eur. Assoc. Pet. Geosci., vol. 4, edited by A. Mascle, pp. 269–280, Springer, New York.

Eltchaninoff-Lancelot, C., S. Triboulet, B. Doudoux, S. Fudral, J. P. Rampnoux, and M. Tardy (1982), Stratigraphie et tectonique des unités delphino-helvétiques comprises entre Mont-Blanc et Belledone (Savoie–Alpes occidentales): Implications régionales, *Bull. Soc. Geol. Fr.*, *XXIV*, 817–830.

Epard, J. L. (1986), Le contact entre le socle du Mont-Blanc et la zone de Chamonix: Implications tectoniques, *Bull. Soc. Vaudoise Sci. Nat.*, *78*, 225–245.

Epard, J. L. (1990), La nappe de Morcles au Sud-Ouest du Mont-Blanc, *Mém. Géol. Lausanne*, *8*, 165 pp.

Escher, A., H. Masson, and A. Steck (1988), Coupes géologiques des Alpes occidentales suisses, Serv. Hydrol. et Géol. Natl., Bern.

Escher, A., H. Masson, and A. Steck (1993), Nappe geometry in the western Swiss Alps, *J. Struct. Geol.*, *15*, 501–509.

Fabre, C., M. C. Boiron, J. Dubessy, M. Cathelineau, and D. A. Banks (2002), Palaeofluid chemistry of a single fluid event: A bulk and in-situ multi-technique analysis (LIBS, Raman spectroscopy) of an Alpine fluid (Mont-Blanc), *Chem. Geol.*, *182*, 249–264.

Fügenschuh, B., and S. M. Schmid (2003), Late stages of deformation and exhumation of an orogen constrained by fission-track data: A case study in the western Alps, *Geol. Soc. Am. Bull.*, *115*, 1425–1440.

Galbraith, R. F. (1981), On statistical models for fission track counts, *Math. Geol.*, *13*, 471–478.

Gidon, M. (2001), Les massifs cristallins externes des Alpes occidentals françaises sont-ils charriés?, *Géol. Alpine*, *77*, 23–38.

Gillcrist, R., M. Coward, and J. L. Mugnier (1987), Structural inversion and its controls: Examples from the Alpine foreland and the French Alps, *Geodin. Acta*, *1*, 5–34.

Gourlay, P. (1983), Le jeu décrochant dextre tardif de la suture de Chamonix (Alpes françaises et suisses), *C. R. Acad. Sci., Ser. 2*, *296*, 927–932.

Gourlay, P. (1986), La déformation du socle et des couvertures delphino-helvétiques dans la région du Mont-Blanc (Alpes occidentales), *Bull. Soc. Geol. Fr., Ser. II*, *8*, 159–169.

Grasmück, K. (1961), Die helvetishen Sedimente am Nordostrand des Mont-Blanc-Massivs (zwishen Sembrancher und dem Col Ferret), *Eclogae Geol. Helv.*, *54*, 351–450.

Green, P. F. (1981), A new look at statistics in fission track dating, *Nucl. Tracks Radiat. Meas.*, *5*, 77–86.

Green, P. F., I. R. Duddy, A. J. W. Gleadow, and J. F. Lovering (1989a), Apatite fission-track analysis as a paleotemperature indicator for hydrocarbon exploration, in *Thermal History of Sedimentary Basins: Methods and Case Histories*, edited by N. D. Naeser and T. H. McCulloh, pp. 181–195, Springer, New York.

Green, P. F., I. R. Duddy, G. M. Laslett, K. A. Hegarty, A. J. W. Gleadow, and J. F. Lovering (1989b), Thermal annealing of fission-tracks in apatite, 4, Quantitative modelling techniques and extension to geological timescales, *Chem. Geol.*, *79*, 155–182.

Guellec, S., J.-L. Mugnier, M. Tardy, and F. Roure (1990), Neogene evolution of the western Alpine foreland in the light of ECORS data and balanced cross-section, in *Deep structure of the Alps*, edited by F. Roure, P. Heitzmann, and R. Polino, *Mem. Soc. Geol. Fr.*, *156*, 165–184.

Guermani, A., and G. Pennacchioni (1998), Brittle precursors of plastic deformation in a granite: An example from the Mont-Blanc massif (Helvetic, western Alps), *J. Struct. Geol.*, *20*, 135–148.

Harrison, T. M., R. L. Amstrong, and G. K. C. Clarke (1978), Thermal models and cooling histories from fission-track, K-Ar, Rb-Sr and U-Pb mineral dates, northern coast plutonic complex, British Columbia, in *Fourth International Conference on Geochronology, Cosmochronology, and Isotope Geology*, edited by R. E. Zartman, *U.S. Geol. Surv. Open File Rep.*, *78-701*, 167–170.

Harrison, T. M., M. T. Heizler, O. M. Lovera, W. Chen, and M. Grove (1994), A chlorine disinfectant for excess argon released from K-feldspar during step heating, *Earth Planet. Sci. Lett.*, *123*, 95–104.

Hubbard, M., and N. S. Mancktelow (1992), Lateral displacement during Neogene convergence in the western and central Alps, *Geology*, *20*, 943–946.

Huon, S., M. Burkhard, and J. C. Hunziker (1994), Mineralogical, K/Ar, stable and Sr isotope systematics of K-white micas during very low grade metamorphism of limestones (Helvetic nappes, western Switzerland), *Chem. Geol.*, *113*, 347–376.

Hurford, A. J. (1986), Cooling and uplift patterns in the Lepontine Alps south central Switzerland and age of vertical movement on the Insubric fault line, *Contrib. Mineral. Petrol.*, *92*, 423–427.

Jan du Chêne, R. (1974), Etude palynologique du Néogène et du Pléistocène inférieur de Bresse (France), Ph.D. thesis, Univ. de Genève, Geneva, Switzerland.

Ketcham, R. A., R. A. Donelick, and W. D. Carlson (1999), Variability of apatite fission-track annealing kinetics: III. Extrapolation to geological time scales, *Am. Mineral.*, *84*, 1235–1255.

Kirschner, D. L., Z. D. Sharp, and H. Masson (1995), Oxygen isotope thermometry of quartz-calcite veins: Unraveling the thermal-tectonic history of the subgreenschist facies Morcles nappe (Swiss Alps), *Geol. Soc. Am. Bull.*, *107*, 1145–1156.

Kirschner, L., M. A. Cosca, H. Masson, and J. C. Hunziker (1996), Staircase $^{40}Ar/^{39}Ar$ spectra of fine-grained white mica: Timing and duration of deformation and empirical constraints on argon diffusion, *Geology*, *24*, 747–750.

Krummenacher, D., and J. Evernden (1960), Détermination d'âge isotopique faites sur quelques roches des Alpes par la méthode Potassium-Argon, *Schweiz. Miner. Petrogr. Mitt.*, *40*, 267–277.

Lacassin, R., P. Tapponnier, and L. Bourjot (1990), Culminations d'échelle crustale et imbrication de la lithosphère dans les Alpes, apports du profil ECORS-CROP, *C. R. Acad. Sci., Ser. II*, *310*, 807–814.

Leloup, P. H., N. Arnaud, R. Lacassin, J. R. Kienast, T. M. Harrison, P. T. Trinh, A. Replumaz, and P. Tapponnier (2001), New constraints on the structure, thermochronology and timing of the Ailao Shan–Red River shear zone, SE Asia, *J. Geophys. Res.*, *106*, 6683–6732.

Lemoine, M., P. C. d. Graciansky, and P. Tricart (2000), *De l'Océan à la Chaîne de Montagnes–Tectonique des Plaques des Alpes*, 207 pp., Gordon and Breach, New York.

Leutwein, F., B. Poty, J. Sonet, and J.-L. Zimmermann (1970), Age des cavités à cristaux du granite du Mont-Blanc, *C. R. Acad. Sci., Ser. D*, *271*, 156–158.

Lovera, O. M., F. M. Richter, and T. M. Harrison (1991), Diffusion domains determined by ^{39}Ar released during step heating, *J. Geophys. Res.*, *96*, 2057–2069.

Marshall, D., D. Kirschner, and F. Bussy (1997), A variscan pressure-temperature-time-path for the N-E Mont-Blanc massif, *Contrib. Mineral. Petrol.*, *126*, 416–428.

Marshall, D., N. Meisser, and R. P. Taylor (1998a), Fluid inclusion, stable isotope and Ar-Ar evidence for the age and origin of gold-bearing quartz veins at Mont Chemin, Switzerland, *Mineral. Petrol.*, *62*, 147–165.

Marshall, D., H. R. Pfeifer, J. C. Hunziker, and D. Kirschner (1998b), A pressure-temperature-time path for the NE Mont-Blanc massif: Fluid-inclusion, isotopic and thermobarometric evidence, *Eur. J. Mineral.*, *10*, 1227–1240.

Masson, F., F. Gal, and P. H. Leloup (2002), Une carte gravimétrique haute résolution du massif du Mont-Blanc: Implications structurales, *C. R. Geosci.*, *334*, 1011–1019.

Masson, H. (1976), Un siècle de géologie des Préalpes: De la découverte des nappes à la recherche de leur dynamique, *Eclogae Geol. Helv.*, *73*, 331–349.

Mattauer, M. (1986), Les subductions intracontinentales des chaînes tertiaires d'Asie; leurs relations avec les décrochements, *Bull. Soc. Geol. Fr.*, *8*, 143–157.

Ménard, G., and T. F. Thouvenot (1987), Coupes equilibrees crustales; methodologie et application aux Alpes occidentales, *Geodin. Acta*, *1*, 35–45.

Mennessier, G., F. Carme, J. Bellière, R. Dhellemes, P. Antoine, and N. Oulianoff (1976), Geological map of France, scale 1/50,000, sheet St Gervais-les-Bains (703), Bur. de Rech. Geol. et Min., Orléans, France.

Nicolas, A., R. Polino, A. Hirn, R. Nicolich, and ECORS-CROP Working Group (1990), ECORS-CROP traverse and deep structure of the western Alps. A synthesis, in *Deep Structure of the Alps*, edited by F. Roure, P. Heitzmann, and R. Polino, *Mem. Soc. Geol. Fr.*, *156*, 15–27.

Pairis, J. L., et al. (1993), Geological map of France, scale 1/50,000, sheet Cluses (679), Bur. de Rech. Geol. et Min., Orléans, France.

Pfiffner, O. A. (1993), The structure of the Helvetic nappes and its relation to the mechanical stratigraphy, *J. Struct. Geol.*, *15*, 511–521.

Pfiffner, O. A., P. Lehner, P. Heitzmann, S. Müller, and A. Steck (1997), *Deep Structure of the Swiss Alps: Results of NRP 20*, Springer, New York.

Pfiffner, O. A., F. Schlunegger, and S. J. H. Buiter (2002), The Swiss Alps and their peripheral foreland basin: Stratigraphic response to deep crustal processes, *Tectonics*, *21*(2), 1009, doi:10.1029/2000TC900039.

Platt, J. P. (1984), Balanced cross-sections and their implications for the deep structure of the northwest Alps: Discussion, *J. Struct. Geol.*, *6*, 5.

Poty, B., and M. Cathelineau (1999), La formation des cristaux dans les fentes alpines du massif du Mont-Blanc, *Regne Miner., Hors Ser. V*, 19–21.

Poty, B., H. A. Stalder, and A. M. Weisbrod (1974), Fluid inclusions studies in quartz from fissures of western and central Alps, *Schweiz. Mineral. Petrogr. Mitt.*, *54*, 717–752.

Ramsay, J. G. (1981), Tectonics of the Helvetic nappes, in *Thrust and Nappe Tectonics*, edited by K. R. McClay and N. J. Price, *Spec. Publ. Geol. Soc.*, *9*, 293–309.

Renne, P. R., C. C. Swisher, A. L. Deino, D. B. Karner, T. L. Owens, and D. J. DePaolo (1998), Intercalibration of standards, absolute ages and uncertainties in $^{40}Ar/^{39}Ar$ dating, *Chem. Geol.*, *145*, 117–152.

Roddick, J. C., R. A. Cliff, and D. C. Rex (1980), The evolution of excess argon in alpine biotites, a $^{40}Ar/^{39}Ar$ analysis, *Earth Planet. Sci. Lett.*, *48*, 185–208.

Rolland, Y., S. Cox, A.-M. Boullier, G. Pennacchioni, and N. Mancktelow (2003), Rare earth and trace element mobility in mid-crustal shear zones: Insights from the Mont Blanc Massif (western Alps), *Earth Planet. Sci. Lett.*, *214*, 203–219.

Rossi, M., Y. Rolland, O. Vidal, and S. F. Cox (2005), Geochemical variations and element transfer during shear zone development and related episyenites at middle crust depths: Insights from the Mont-Blanc granite (French-Italian Alps), in *High Strain Zones: Structure and Physical Properties*, edited by D. Brunh and L. Burlini, *Geol. Soc. Spec. Publ.*, in press.

Ruffini, R., M. Cosca, A. d'Atri, J. C. Hunziker, and R. Polino (1995), The volcanic supply of the Taveyanne turbidites (Savoie, France): A riddle for Tertiary Alpine volcanism, *Atti Accad. Sci. Roma*, *14*, 359–376.

Schmid, S. M., and E. Kissling (2000), The arc of the western Alps in the light of geophysical data on deep crustal structure, *Tectonics*, *19*, 62–85.

Seward, D., and N. S. Mancktelow (1994), Neogene kinematics of the central and western Alps: Evidence from fission-track dating, *Geology*, *22*, 803–806.

Sobel, E. R., and M. R. Strecker (2003), Uplift, exhumation, and precipitation: Tectonic and climatic control of Late Cenozoic landscape evolution in the northern Sierras Pampeanas, Argentina, *Basin Res.*, *15*, doi:10.1046/j.1365-2117.2003.00214.x.

Soom, M. A. (1990), Abkühlungs- und Hebungsgeschichte der Externmassive und der Penninischen decken beidseits der Simplon-Rhone-Linie seit dem Oligozän: Spaltspurdatierungen an apatit/zirkon und K/Ar-datierungen an biotit/muskowit (westliche zentralalpen), Ph.D. thesis, 119 pp., Univ. of Bern, Bern.

Sue, C., and P. Tricart (2003), Neogene to ongoing normal faulting in the inner western Alps: A major evolution of the late alpine tectonics, *Tectonics*, *22*(5), 1050, doi:10.1029/2002TC001426.

Thouvenot, F., J. Fréchet, L. Jenatton, and J.-F. Gamond (2003), The Belledonne border fault: Identification of an active seismic strike-slip fault in the western Alps, *Geophys. J. Int.*, *155*, 174–192.

Vigny, C., et al. (2002), GPS network monitors the western Alps over a five year period: 1993–1998, *J. Geod.*, *76*, 63–76.

Von Raumer, J. F. (1967), Zur Metamorphose amphibolitisher Gesteine im Altkristallin des Mont-Blanc und Aiguilles Rouges Massivs, *Schweiz. Mineral. Petrogr. Mitt.*, *54*, 471–488.

Von Raumer, J. F. (1974), Kristallization und gefügebildung im Mont-Blanc granit, *Schweiz. Mineral. Petrogr. Mitt.*, *47*, 499–579.

Von Raumer, J. F., and F. Neubauer (Eds.) (1993), *Pre-Mesozoic Geology in the Alps*, Springer, New York.

Von Raumer, J. F., J. Abrecht, F. Bussy, B. Lombardo, R.-P. Ménot, and U. Schaltegger (1999), The Palaeozoic evolution of the external massifs, *Schweiz. Mineral.Ppetrogr. Mitt.*, *79*, 5–22.

N. Arnaud, Laboratoire de Dynamique de la Lithosphère (LDL), UMR CNRS 5573, ISTEEM-USTL, Place Eugène Bataillon, F-34095 Montpellier Cedex 5, France.

R. Lacassin, Laboratoire de Tectonique, Mécanique de la Lithosphère, UMR CNRS 7578, Institut de Physique du Globe de Paris, 4 place Jussieu, F-75252 Paris Cedex 05, France.

P. H. Leloup, Laboratoire des Sciences de la terre, UMR CNRS 5570, Université Claude Bernard, 2 rue Raphaël Dubois, F-69622 Villeurbanne Cedex, France. (herve.leloup@univ-lyon1.fr)

E. R. Sobel, Institut für Geowissenschaften, Universität Potsdam, Postfach 60 15 53, D-14415 Potsdam, Germany.

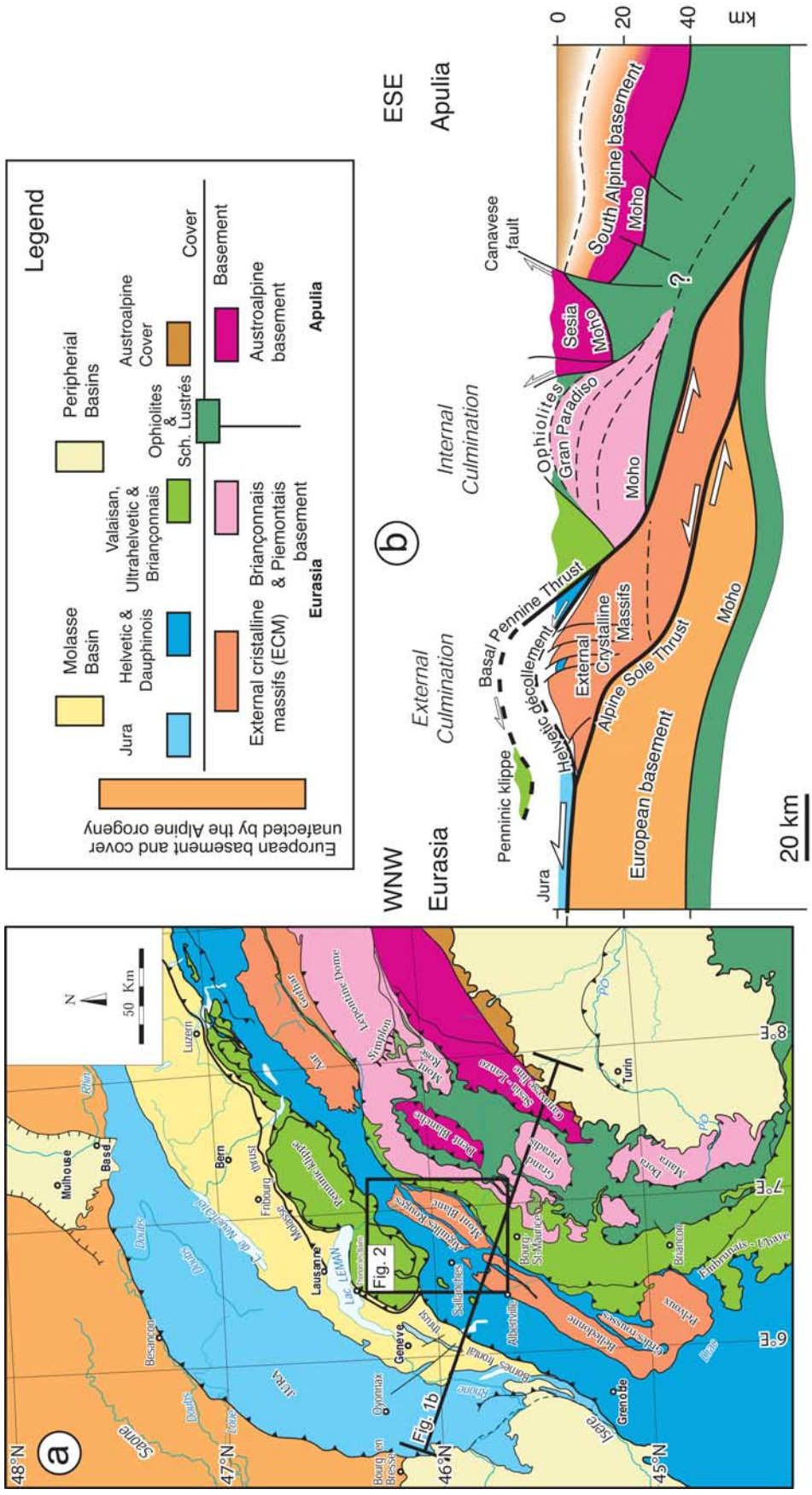

Figure 1. Structural framework of the western Alps. Legend is for both Figures 1a and 1b. (a) Structural map of the western Alps. (b) Large-scale geological cross section of the western Alps. Modified from *Lacassin et al.* [1990].

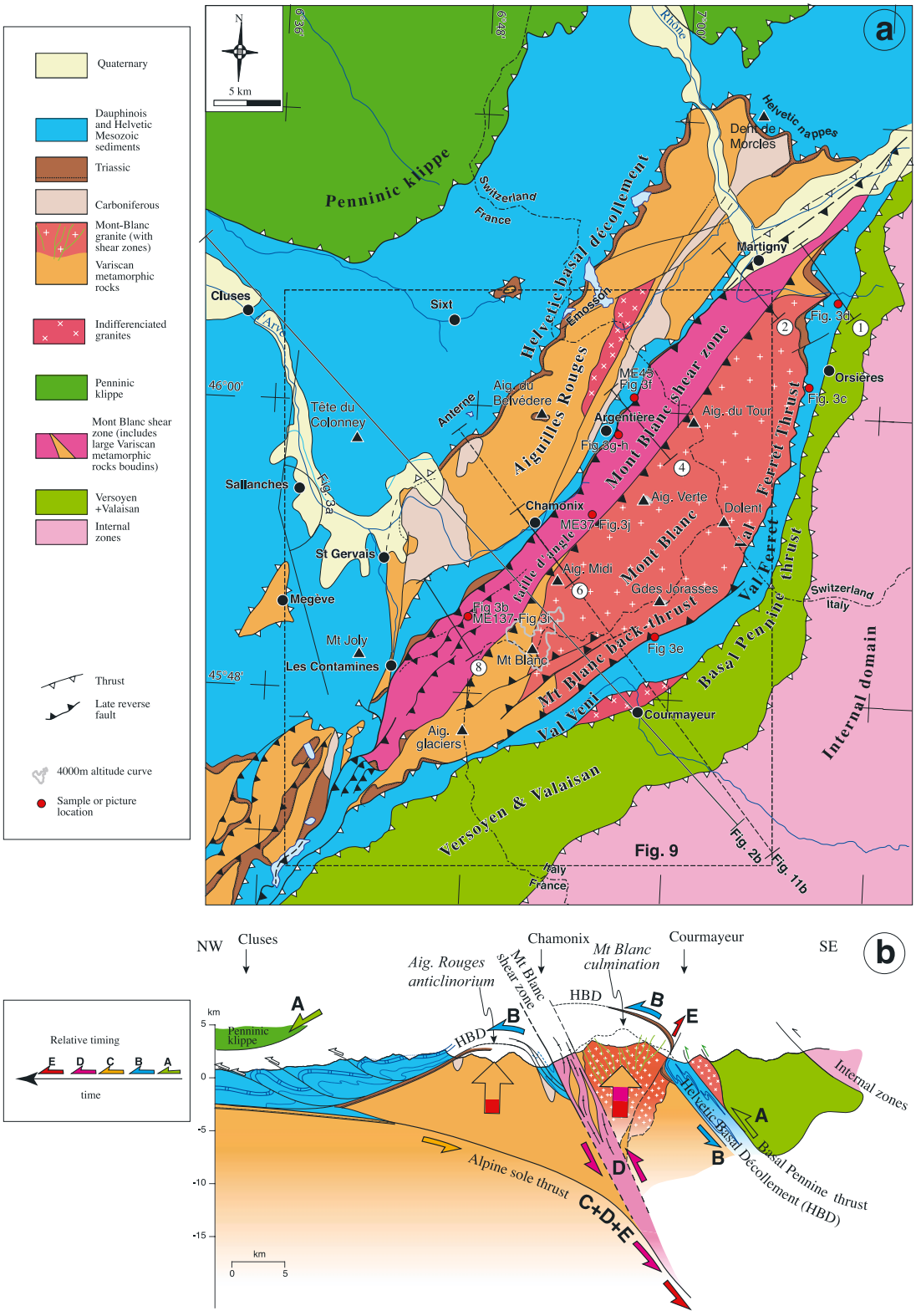
Quaternary
Dauphinois and Helvetic Mesozoic sediments
Triassic
Carboniferous
Mont-Blanc granite (with shear zones)
Variscan metamorphic rocks
Indifferenciated granites
Penninic klippe
Mont Blanc shear zone (includes large Variscan metamorphic rocks boudins)
Versoyen +Valaisan
Internal zones
Thrust
Late reverse fault
4000m altitude curve
Sample or picture location
N
5 km
a
Penninic klippe
Switzerland
France
Helvetic basal décollement
Dent de Morcles
Helvetic nappes
Martigny
Cluses
Sixt
Emosson
Fig. 3d
Orsières
Fig. 3c
Aiguilles Rouges
Mont Blanc shear zone
Val Ferret Thrust
ME45 Fig. 3f
Aig. du Belvédere
Argentière
Fig.3g-h
Aig. du Tour
Arve
Arpette
Tête du Colonney
Sallanches
Fig. 3a
Chamonix
ME37-Fig.3j
Aig. Verte
Dolent
Mont Blanc
Val Ferret thrust
St Gervais
Aig. Midi
Gdes Jorasses
Megève
Fig 3b
ME137-Fig.3i
Switzerland
Italy
Mt Joly
Les Contamines
Mt Blanc
Fig 3e
Mt Blanc back-thrust
Basal Penninic thrust
Internal domain
Val Veni
Courmayeur
Aig. glaciers
Versoyen & Valaisan
Fig. 9
Fig. 2b
Fig. 11b
Italy
France
46°00'
45°48'
b
NW
Cluses
Chamonix
Courmayeur
SE
Aig. Rouges anticlinorium
Mt Blanc shear zone
Mt Blanc culmination
HBD
Penninic klippe
Internal zones
Helvetic Basal Décollement (HBD)
Basal Pennine thrust
Alpine sole thrust
C+D+E
Relative timing
E D C B A
time
km

Figure 2

Figure 2. Structure of the Mont Blanc massif. (a) Structural map of the Mont Blanc massif. The map is drawn from published geological maps: Mont Blanc [*Antoine et al.*, 1979]; Chamonix [*Bellière et al.*, 1987]; Cluses [*Pairis et al.*, 1993], and St. Gervais-les-Bains [*Mennessier et al.*, 1976], as well as personal observations. (b) Synthetic cross section of the Mont Blanc massif. On the basis of our observations (see also Figure 5), HBD is the Helvetic basal décollement. Note that this section is compatible with recent gravity data of the area [*Masson et al.*, 2002]. See section 3.6 for discussion on the relative timing of deformation events.

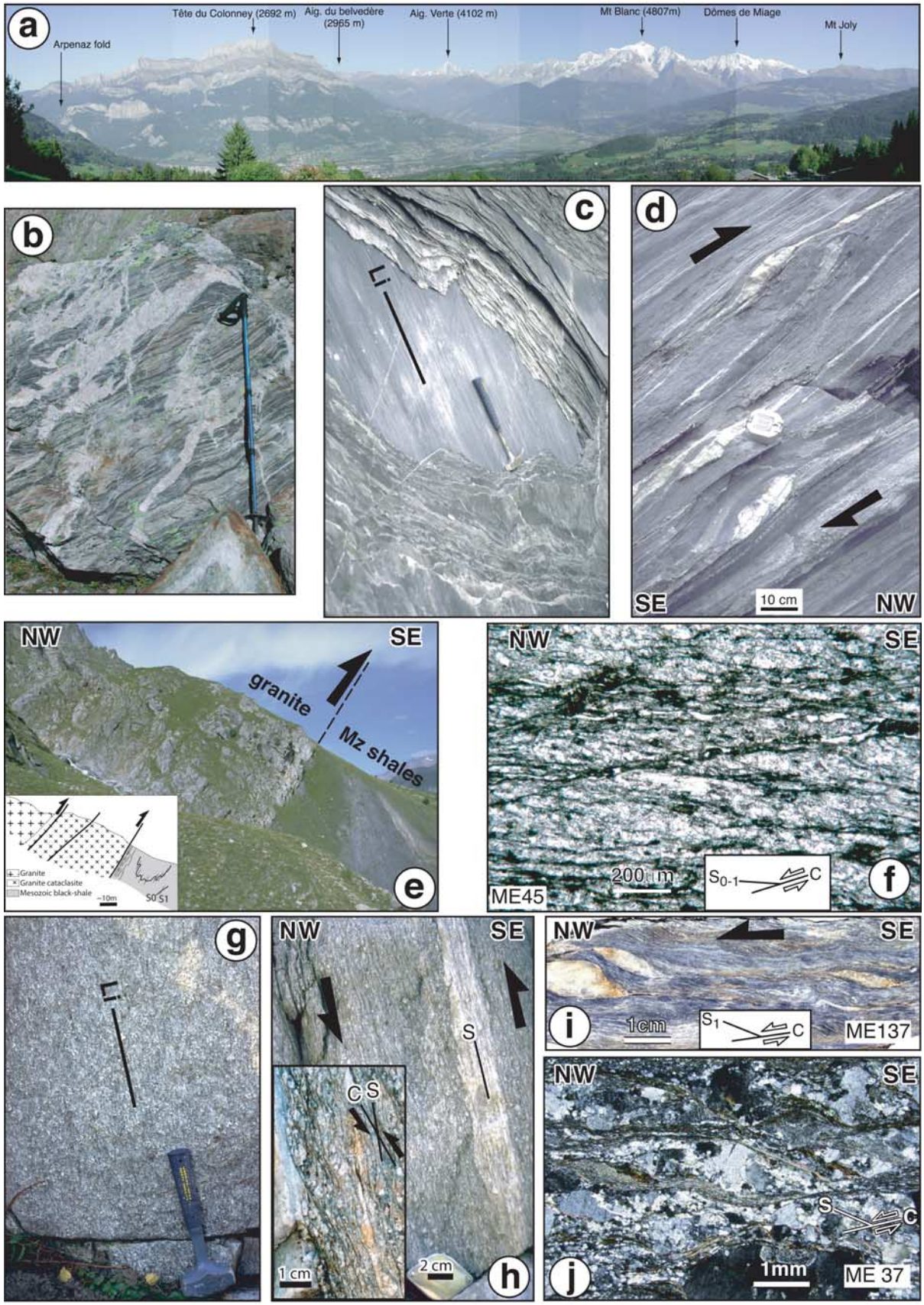
a
Arpenaz fold
Tête du Colonney (2692 m)
Aig. du belvedère (2965 m)
Aig. Verte (4102 m)
Mt Blanc (4807m)
Dômes de Miage
Mt Joly
b
c
Li
d
SE
10 cm
NW
NW
SE
granite
Mz shales
Granite
Granite cataclasite
Mesozoic black-shale
~10m
S0 S1
e
NW
SE
200 µm
ME45
S0-1
C
f
g
Li
NW
SE
S
C S
1 cm
2 cm
h
NW
SE
1cm
S1
C
ME137
i
NW
SE
S
C
1mm
ME 37
j

Figure 3

Figure 3. Deformation in the Mont Blanc massif. For pictures locations see Figure 2a. (a) High glaciated peaks of the Mont Blanc massif viewed from the WNW; view from Cordon, above Sallanches. This landscape is an oblique view of the central part of the section shown in Figure 2b. (b) Aplitic veins intruding the Variscan gneisses; SW part of the Mont Blanc massif, above the Nid d'Aigle. (c) Schistosity and stretching lineation in Liassic shales in Combes des fonds of the Swiss Val Ferret, corresponding to the root of the Helvetic nappes. Li indicates the lineation direction (see Figure 4a). Hammer gives scale. (d) Sheared calcite veins in Liassic shales of the Swiss Val Ferret indicating top to the NW thrusting. Compass gives scale. (e) Back thrusting of the Mont Blanc granite on top of the steepened Liassic series of the Italian Val Ferret. Picture is from the pathway to the Bocallette refuge, south of the Grandes Jorasses. The inset is the corresponding cross section. (f) Thin section of Mesozoic calcschists of the Chamonix syncline. Vormaine ridge, near Le Tour (see Figure 5c). The rock shows a strong schistosity (N21°, 57°E) and lineation (pitch 72°N) (Figure 4c). The shear planes (C) indicate a top to the NW sense of shear parallel to motion in Mont Blanc shear zone (Figure 4c and 4d). (g) Alpine stretching lineation in othogneissess (Ordovician protolith) east of Argentière. Foliation is N15°, 67°E, and lineation pitch is 77°N (see Figure 4d). (h) Sheared aplitic vein in the Argentière orthogneisses. The inset shows C/S structures in orthogneiss. C planes shallower than the foliation indicate thrusting to the NW. (i) Polished slab of sample ME137 from an alpine shear zone affecting the Variscan gneiss. Foliation is N60°, 48°S, and lineation pitch is 75°E. C/S relationships indicate thrusting to the NW. (j) Thin section of sample ME37, Echelles du Montenvers. Foliation is N20°, 65°S, and lineation pitch is 90°. C/S relationships indicate thrusting to the NW.

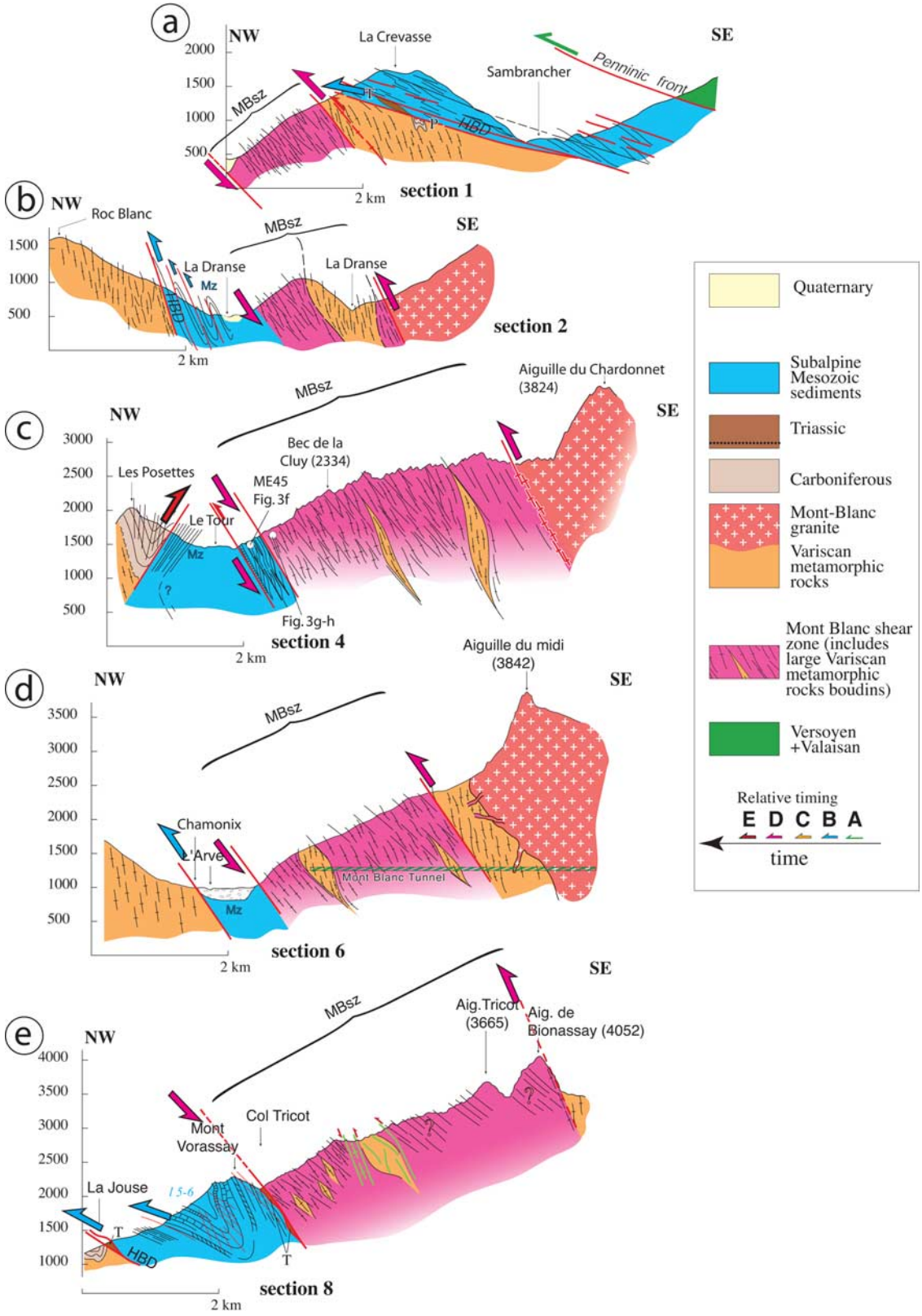

Figure 5. Cross sections of the NW flank of the Mont Blanc massif. NW-SE cross sections from the northern to the southern extremity of the massif (sections 1 to 8, respectively). See Figure 2a for locations. No vertical exaggeration. Mz and l 5–6 refer to Mesozoic sediments and T refers to Triassic sandstones.

Figure 12. Structural evolution of the external Alps. (a–g) Structural evolution of the external Alps along a NW-SE section across the Aiguilles Rouges and Mont Blanc massifs, depicted seven time steps from 50 Ma to present-day. Note that the structural evolution of the internal Alps, mostly occurring before 32 Ma, is not depicted. Shortening estimates in the Jura and Helvetic nappes from *Affolter* [2003]. A to D refer to the main deformation phases in the Aiguilles Rouges and Mont Blanc massifs (see also Figures 2b and 8). Note that the bottom line of the section does not correspond to the Moho but rather to a passive marker at the top of the layered lower crust. (h) ECORS-CROP seismic line for broad comparison with Figure 12g [from *Schmid and Kissling*, 2000]. Some structures, such as the Mont Blanc back thrust, are offset from this seismic line, which goes through Belledonne south of the Mont Blanc (see Figure 1a).

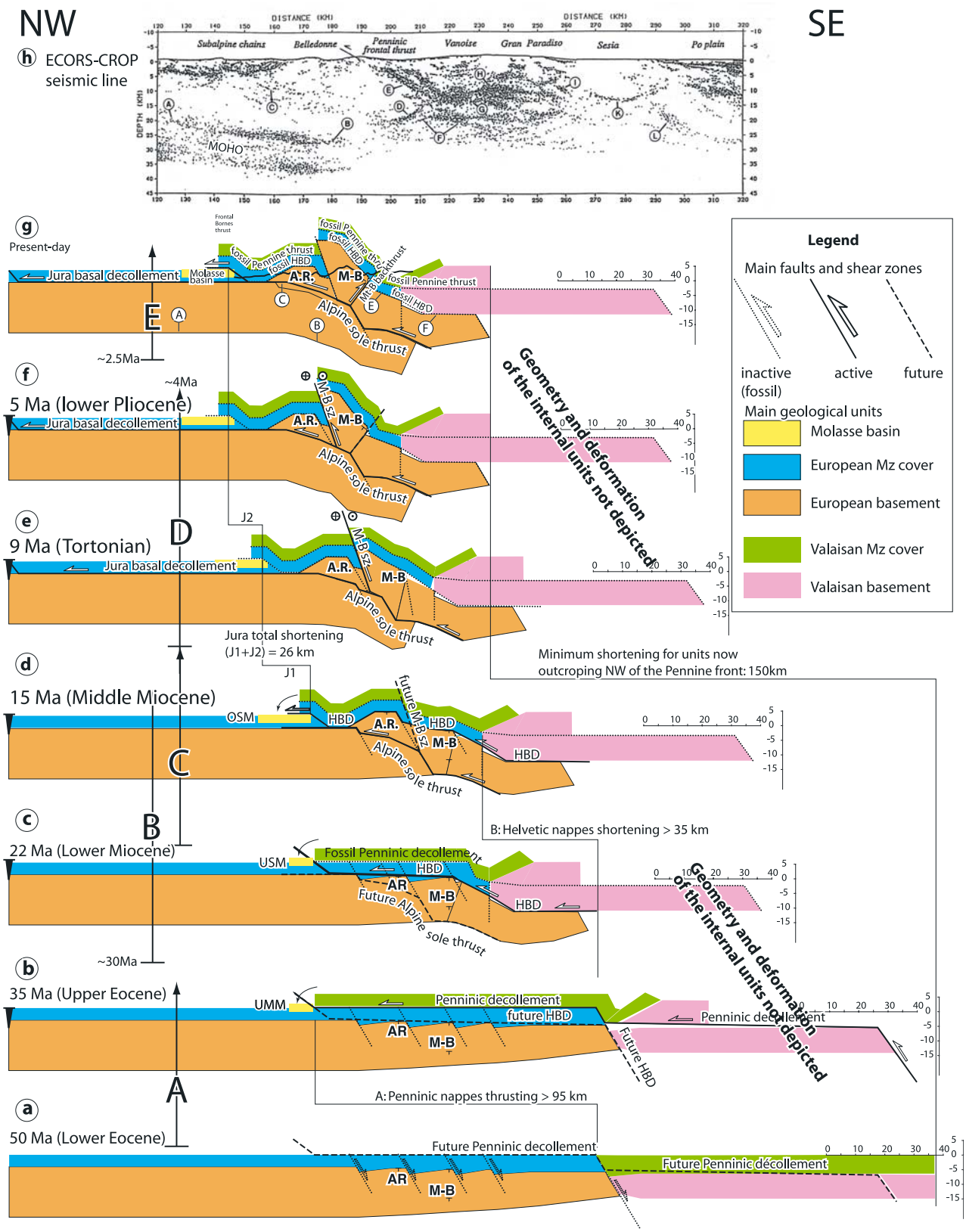
NW
SE
h ECORS-CROP seismic line
DISTANCE (KM)
DEPTH (KM)
Subalpine chains
Belledonne
Penninic frontal thrust
Vanoise
Gran Paradiso
Sesia
Po plain
MOHO
g
Present-day
Jura basal decollement
Molasse basin
fossil Penninic thrust
fossil HBD
A.R.
M-B
M-B backthrust
fossil Pennine thrust
Alpine sole thrust
~2.5Ma
f
~4Ma
5 Ma (lower Pliocene)
M-B sz
e
9 Ma (Tortonian)
J2
Jura total shortening
(J1+J2) = 26 km
d
15 Ma (Middle Miocene)
J1
OSM
HBD
future M-B sz
c
22 Ma (Lower Miocene)
USM
Fossil Penninic decollement
Future Alpine sole thrust
~30Ma
b
35 Ma (Upper Eocene)
UMM
Penninic decollement
future HBD
Future HBD
a
50 Ma (Lower Eocene)
Future Penninic decollement
Future Penninic décollement
A
B
C
D
E
Geometry and deformation of the internal units not depicted
Minimum shortening for units now outcroping NW of the Pennine front: 150km
B: Helvetic nappes shortening > 35 km
A: Penninic nappes thrusting > 95 km
Legend
Main faults and shear zones
inactive (fossil)
active
future
Main geological units
Molasse basin
European Mz cover
European basement
Valaisan Mz cover
Valaisan basement

Figure 12